PATHOGEN DETECTION LAB-ON-A-CHIP (PADLOC) SYSTEM FOR PLANT PATHOGEN DIAGNOSIS

A Thesis

by

OSMAN SAFA CIFCI

Submitted to the Office of Graduate Studies of
Texas A&M University
in partial fulfillment of the requirements for the degree of

MASTER OF SCIENCE

August 2012

Major Subject: Electrical Engineering

Pathogen Detection Lab-on-a-Chip (PADLOC) System for Plant Pathogen Diagnosis

PATHOGEN DETECTION LAB-ON-A-CHIP (PADLOC) SYSTEM FOR PLANT PATHOGEN DIAGNOSIS

A Thesis

by

OSMAN SAFA CIFCI

Submitted to the Office of Graduate Studies of
Texas A&M University
in partial fulfillment of the requirements for the degree of

MASTER OF SCIENCE

Approved by:

Chair of Committee,	Arum Han
Committee Members,	Xing Cheng
	Jim Ji
	Won-Bo Shim
Head of Department,	Costas N. Georghiades

August 2012

Major Subject: Electrical Engineering

ABSTRACT

Pathogen Detection Lab-On-A-Chip (PADLOC) System for Plant Pathogen Diagnosis.

(August 2012)

Osman Safa Cifci, B.S., Eskisehir Osmangazi Univertsity

Chair of Advisory Committee: Dr. Arum Han

Polymerase Chain Reaction (PCR) detection paves the way to reliable and rapid diagnosis of diseases and has been used extensively since its introduction. Many miniaturized PCR systems were presented by microfluidics and lab-on-a-chip community. However, most of the developed systems did not employ real-time detection and thus required post-PCR processes to obtain results. Among the few real-time PCR systems, almost all of them aimed for medical applications and those for plant pathogen diagnosis systems are almost non-existent in the literature.

In this work, we are presenting a portable system that employs microfluidics PCR system with integrated optical systems to accomplish real-time quantitative PCR for plant pathogen diagnosis. The system is comprised of a PCR chip that has a chamber for PCR sample with integrated metal heaters fabricated by standard microfabrication procedures, an optical system that includes lenses, filters, a dichroic mirror and a photomultiplier tube (PMT) to achieve sensitive fluorescence measurement capability and a computer control system for Proportional Integral Derivative (PID) control and data acquisition. The optical detection system employs portable components and has a size of 3.9 x 5.9 x 11.9 cm which makes it possible to be used in field settings. On the

device side, two different designs are used. The first design includes a single chamber in a 25.4 x 25.4 mm device and the capacity of the chamber is 9 µl which is sufficient to do gel electrophoresis verification. The second design has three 2.2 µl chambers squeezed in the same size device while having smaller volume to increase high throughput of the system.

The operation of the system was demonstrated using Fusarium oxysporum spf. lycopersici which is a fungal plant pathogen that affects crops in the USA. In the presence of the plant pathogen, noticeable increases in the photomultiplier tube output were observed which means successful amplifications and detections occurred. The results were confirmed using gel electrophoresis which is a conventional post-PCR process to determine the existence and length of the amplified DNA. Clear bands located in the expected position were observed following the gel electrophoresis.

Overall, we have presented a portable PCR system that has the capability of detecting plant pathogens.

DEDICATION

To my dear family and friends for your unconditional love and support

ACKNOWLEDGEMENTS

I would like to thank my advisor and committee chair, Dr. Arum Han, for his unwavering guidance and support all the way. I would like to thank my committee members, Dr. Xing Cheng, Dr. Jim Ji, and Dr. Won-Bo Shim as well as Dr. Jun Zou for their advice and support. My special thanks go to Dr. Shim for kindly providing me with the opportunity to work in his lab.

I would like to thank my collaborator, Martha, for her patient tutorials and generous help. I also want to thank my group members, Jaewon Park, Hyunsoo Kim, Chiwan Koo, Han Wang, Celal Erbay, Haron Abdel-Raziq and Adrian Guzman, and alumni Huijie Hou, Whitney Parker, and Jianzhang Wu for their enormous help in the lab and in life. I would especially like to state my appreciation to Chiwan and Hyun Soo for their involvement in the PADLOC project.

Life without Celal Erbay, Haron Abdel-Raziq and my roommate Ahmad Bashaireh in College Station would definitely be an unpleasant experience. Thank you all for offering your kind friendship.

TABLE OF CONTENTS

Page

Page

LIST OF FIGURES

Page

Page

Page

LIST OF TABLES

Page

CHAPTER I

INTRODUCTION

1.1. Objective and Motivation for Plant Pathogen Detection

Plant diseases result in billions of dollars loss every year to agriculture, landscape and forestry in the United States.[1] The reasons for economic losses are reduction in the quality of the products, yield, aesthetic and nutritional value as well as contamination of food via toxic means. Additionally, proper maintaining the land paves the way to keeping and even increasing the food supplies while increasing the cultivated land minimally. By managing the land, it is possible to protect the domestic crops against foreign diseases and increase the export market for plant products. There is a need for rapid and accurate detection of plant pathogen in order to avoid big economic losses in crops. The control of a plant disease involves identifying the disease or finding the pathogen causing the disease. There are many known pathogens and diseases by scientist and the number of these increases by the introduction of emerging diseases caused by previously unknown pathogen or mutation of known pathogens.

Previously, the pathogens used to be detected by in-vitro screens, microscopic examination and biochemical tests. These methods take long time, require a specialist or expensive materials. Therefore; new, sensitive, accurate, portable and inexpensive methods are required for plant pathogen detection. The DNA based detection methods are on the rise and are expected to be used to identify more and more pathogens. One of

---

This thesis follows the style of *Lab Chip*.

the most commonly used DNA based diagnosis method is polymerase chain reaction (PCR).[2] As PCR becomes more and more common in the laboratory settings, the lab-on-a-chip community presents more and more PCR systems that employ unique properties of miniaturized systems. There are many miniaturized PCR systems developed in the literature. However, most of the PCR work did not employ real-time detection of PCR product and relied on post-PCR procedures. Out of the real-time PCR systems were intended for medical field and real-time PCR detection for plant diseases are almost non-existent in the literature. The motivation for this study is the development of a portable plant pathogen detection system that employs polymerase chain reaction to amplify target pathogens and at the same time detect the presence or absence of the target pathogen that could be used in a field setting.

1.2. Conventional PCR Systems

The polymerase chain reaction (PCR) is a very useful laboratory tool that selectively replicates DNA and is used in crop pathogen detection, clinical medicine, genetic disease identification, forensics science among others. Since its introduction to scientific literature,[2] the method of amplifying a specific sequence has attracted much attention. The very first PCR experiments used to be very laborious because of the requirement of fresh enzyme addition during the run. However, this did not take long and PCR protocol was automated with the introduction of DNA polymerase obtained by thermophiles by Lawyer.[3] This was the breakthrough that renders PCR impossible to ignore.

In the conventional case, PCR involves a temperature cycling of three different temperatures in order to copy DNA. For the DNA replication to occur there are some reaction components that need to exist in the sample. These are water, PCR reaction buffer that usually contains magnesium chloride ($MgCl_2$) to provide an ideal pH and salt environment for the reaction to occur, deoxynucleotide triphosphates (dNTPs) that are individual components that stick during the replication, reverse and forward PCR primers that supply templates for new copies of DNA and lastly DNA polymerase enzyme bring together the components for a successful DNA copy.

As mentioned above, PCR typically requires three different temperature zones. The first step is called denaturation which alters double-stranded DNA into single stranded DNA. The temperature for denaturation is usually approximately 95°C.[4] Afterwards, the sample is cooled down to 48-74°C to let the primers in the sample to anneal to denatured DNAs. This temperature range is referred to as annealing temperature and it is directly related to the melting temperature of the primers. It is very important to determine a working temperature range since too low annealing temperature leads to random amplification of DNAs (losing the specificity) whereas too low annealing temperature results in insufficient products. The last temperature zone in the PCR is called extension where oligonucleotides are extended with the inclusion of deoxynucleotides by the polymerase enzyme. The extension temperature is approximately 72°C. This sequence is repeated for 20 to 45 cycles to ensure having enough DNA replicates.

The research on PCR has continued and more advanced PCR protocols have developed. Traditionally, after the completion of PCR the samples are loaded into a gel medium that contains ethidium bromide to stick to DNA. The gel undergoes potential difference which moves DNA from negative side to positive side since DNA is negatively charged. This post-PCR procedure could be by-passed by employing what is called real-time PCR.[5,6] Real-time PCR refers to using a fluorescence dyes or beacons that intercalate with double-stranded DNA and monitor the increase in fluorescence. Since the increase in fluorescence stems from the increased amount of DNA real-time PCR allows detection as well as quantification of DNA.

Both conventional and real-time PCR are conventionally are used in commercial devices. The conventional PCR machine where only the heating up and cooling down of samples occurs is also called thermocycler. On the other hand, the real-time PCR machine has a fluorescence detection module in addition to thermocycler with an interface on personal computer. These machines are commonly used laboratories but they are bulky and, especially for the case of real-time PCR machine, expensive.

1.3. Microchip PCR Systems

1.3.1. First Miniaturization Efforts

The miniaturization of PCR systems were driven by the potential of reduced cost, decreased reaction times, decreased required PCR sample volume and increased portability.[7] The first miniaturize PCR device came in 1993 by Northrup et al.[8] It was a

silicon-based static chamber design. The device paved the road for more complicated and more functional devices. The first PCR chip along with capillary electrophoresis (CE) approach was published three years after however both protocols did not take place in one chip.[9] Moreover, the first integration of PCR with DNA hybridization on a chip dated back to 2000.[10] The first miniaturized system real-time PCR system came five years after the introduction of real-time PCR.[11] The system was not a fully portable system since it used a fluorescence microscope however the silicon PCR chip was able to replace a thermocycler. The fluorescent dye used is TaqMan probe and samples using SYBR Green as fluorescent dye started coming one year after.[12]

1.3.2. Stationary PCR

The stationary PCR refers to microchip PCR systems where the thermocycling takes place in a stationary chamber and the chamber is heated to different temperature zones. The system looks similar to a conventional PCR system where the samples are filled into plastic tubes and exposed to different temperatures for amplification. The first microchip PCR[7] had a stationary chamber with a 50 µl sample volume which was four times faster and more power efficient than the conventional PCR systems at that time. A big advantage of stationary PCR is that it is a well-characterized system and the fluidic and thermal control is easier than the other system. However, in the case of single stationary PCR chamber the high-throughput is not possible since only one sample can be run at a time.

The throughput of the system can be increased by introducing multiple chambers. By this addition it is possible to employ multiplex detection and reduce the total operation time to a fraction. The material cost of the PCR chip and the labor can also be significantly reduced with the introduction of multiple chamber stationary PCR system. The first multiple chamber stationary PCR chips started coming in 1997 by two groups.[13,11] There is however several problems associated with multiple chamber designs that need to be taken care of. Firstly, the temperature range within the chambers should be the same otherwise amplification of the sample might not occur or occur to a lesser degree. Secondly, increasing the high-throughput can go hand in hand with decreasing sample volume and this might raise several problems such as adsorption of biological components in the sample to the walls of the chamber and evaporation of the sample.

1.3.3. Continuous-flow PCR

In continuous-flow PCR systems, the sample inside the device is not stationary and it keeps moving to three temperature zones. There are three different temperature zones implemented usually by using three different heaters and the sample keeps travelling inside the device. The main motivations for this type are reduction in the operation time because of the very fast heat transfer and thermal cycling since there is no need for the samples to wait to reach the next temperature zone, low possibility of cross-contamination and potential for inclusion of other analytical systems into the same chip. The challenges for continuous-flow PCR is fixed cycle number because of the device

layout and possible increase in adsorption of the samples compared to the stationary PCR systems.

It is possible to subdivide continuous-flow PCR systems into depending on the design of the chip. These are serpentine rectangular channel devices and circular traversing devices. The first serpentine rectangular channel device came out in1998 by Kopp et al.[14] The channel length was 2.2 m long and the sample went through three temperature zones of 95, 60 and 77°C for 20 times. The flow rate changed between 5.8 and 72.9 nl/s taking times between 18.8 and 1.5 minutes. The reduction in operation duration is very significant and this design was taken and improved by other groups. One notable achievement is by Gascoyne et al,[15] where they include dielectrophoresis-field flow fractionation (DEP-FFF) cell separator, cell isolator and lysis, flow-through PCR and detection for malaria detection. A challenge regarding the rectangular channel serpentine devices is the temperature zone transition is denaturation zone, extension zone and annealing zone and it is possible that while the sample left denaturation zone and advancing to extension zone single stranded DNAs can form double strands with the template strands or their complementary strands. This is where the circular traversing devices come in. These devices have a circular design to expose the sample to denaturation zone, annealing zone and finally extension zone which is the sequence in conventional or stationary chamber PCR systems.[16,17]

1.3.4. Other Types of PCR Systems

An important type of PCR is system is droplet-based PCR. It refers to having the sample in droplet form which is a discrete fluid produced by using two immiscible fluids rather than a having the volume inside an enclosed system such as reaction tube, tubing or microfabricated devices.[18] The droplets are aqueous solution enclosed by oil or solvent. Droplet-based PCR systems offer a bigger automation than other PCR systems because droplets can be generated in a very fast fashion. Usually, the droplets are in micro to nanoliter size and can be produced thousands in quantity in an hour.[19] A big advantage of droplet-based systems is the sample's interaction with its surrounding is limited and this reduces the adsorption of templates, dNTPs and polymerase enzyme which is a concern in chamber based or continuous-flow systems. Another advantage droplet-based PCR systems offer is truly isolation and discrete PCR. In cell analysis, the PCR results in the case of a stationary or droplet-based PCR are averaged results which might not be accurate enough. However, droplet-based PCR can ensure a single cell dropletized PCR and offer more accurate results.

Another type of PCR is convectively-driven PCR which refers to having a thermal gradient forcing the sample travel between hot and cold region.[20] The hot region melts the DNA and cold region copies the target DNA. The first system that employs the convection was done in a Rayleigh-Benard cell[21] where 35 µl sample traversed between 97 and 61°C. The advantages of this system are there is no external force needed to push the sample since the sample travels through the regions by itself and low cost fabrication since it doesn't rely on thermocycling electronics or syringe pumps. A

disadvantage of the system is the convection cell is limited to several μm to several cm since the diffusion for small volumes and non-laminar mixing for large volumes become evident for outside of this range.

1.3.5. Various Heating Methods

There are many types of heating structures employed in PCR systems. It is possible to divide the majority of these systems into two groups: Contact heating and non-contact heating. Contact heating makes use of resistive heating when a voltage is applied across a heating element which is in contact with the PCR components. On the other hand, non-contact heating refers to a design where the heating structure is not in direct contact with the PCR components.

Contact heating systems usually utilize thin-film heater elements or metal blocks to efficiently heat up the system. Thin-film heaters can use metals such as Pt,[22-24] aluminum,[25] silver and palladium,[26] chromium and aluminum[27] and indium tin oxide (ITO)[28] as well as poly-silicon.[29-31] An advantage of thin-film heaters is they do not require additional size but microfabrication is required for thin-film heaters. Metallic blocks and Peltier-effect ceramic blocks are another commonly used contact heating method.[32-34] These systems are robust but they suffer from slow thermocycling profile because of their big thermal mass and they consume more power compared to thin-film heaters and they are much bigger in size. To overcome big cycling time, researchers used more than one heating block to achieve a faster rate.[35,36] In addition to thin-film

heater and heating blocks, commercial thin-film resistors,[37,38] resistive heater coils[39,40] and commercial thermal cyclers[41,42] are also used as contact-based heating elements.

The addition of thermal mass for contact-based systems is a disadvantage to achieve fast cycling times and non-contact heating methods can provide a solution to this problem. One type of non-contact heating is hot air heating which is accomplished by flowing a desired temperature hot air. Since the thermal mass of air is small fast cycling time can be achieved.[43] Infrared light heating is another successful non-contact heating method which used a tungsten lamp which achieved 65 and 20°C/s heating and cooling rates in nanoliter size samples[44] and 35 cycle PCR cycling was finished under 15 minutes by Ferrance et al.[45] Light based heating methods require lenses and filters to avoid intervention the PCR reaction. Another methods for non-contact heating without the use of lamps are induction heating which achieved 6.5 and 4.2°C/s heating and cooling rates without the need for accurate alignment and temperature control system[46] and microwave heating[47,48] which reported milliliter-scale PCR.

Apart from contact and non-contact heating several groups came out with non-conventional methods. A heating method was proposed by Guijt et al.[49] which used chemical and physical processes to heat and cool the PCR sample. The heating was achieved by dissolving sulfuric acid with water and cooling by making use of evaporation of acetone. Hence the system does not need external components to heat up or cool down the system which can reduce the overall size of the system. Another heating method was suggested by applying Joule heating with the help of alternating current to the platinum electrodes that are inside the chamber.[50] In this way, it is

possible to heat the sample directly and the system achieved 15°C/s for both cooling and heating rates.

1.3.6. Integrated Detection Methods

There are many detection methods that are included in PCR systems. Some of them require an additional time after the thermocycling happens while other methods can detect during or at the end of the thermocycling.

One integrated post-PCR detection method is electrophoretic sizing or capillary electrophoresis (CE). This method is done after the PCR cycles are complete and refers to separation of DNA by applying voltage to the sample and the outcome can be observed by exciting the sample and read the fluorescence signal. The resulted electropherogram will display response intensity and time. Hence, the amplified genes and their quantity can be estimated. This method was employed as a miniaturized PCR detection system by some researchers.[51-53]

Another post-PCR detection method is DNA hybridization which can reveal the sequence of the target DNA. The sequencing by hybridization relies on oligonucleotide hybridization to detect the set of components present in the DNA.[54] This method requires immobilization of the DNA on a solid support. This sequence-specific technique was miniaturized by several groups as a post-PCR detection method.[55,56]

A widely employed PCR detection technique is fluorescence detection. In this, a fluorescence probe is added to the sample and increase in fluorescence intensity due to the interaction of probe and DNA of the sample correlates to the increase in the number

of DNAs. A big advantage of fluorescence detection is reduction in the detection time. Unlike in hybridization or CE methods, fluorescence detection can be done in a very short time after the thermocycling or along with thermocycling. It is possible to use an end-point fluorescence detection as well as real-time fluorescence detection. End-point detection refers to reading samples before and after the PCR run and compare these two results.[57,58] However, this method can be regarded as an unreliable method since no data can be obtained during the PCR run. A fluorescence detection method that allows having a fluorescence data at every cycle during the thermo cycling is called real-time fluorescence detection. There are two commonly used fluorescence chemicals in real-time microfluidic PCR systems. These are TaqMan® probe and SYBR® Green dye. TaqMan® probe is complementary to the sequence to be copied and it is labeled with fluorescence reporter and fluorescence quencher on the end parts. In the thermocycling process, the reporter and quencher get separated by the DNA polymerase enzyme and fluorescence intensity increases. These probes are highly specific and sensitive however, long testing and optimization might be needed.[59] SYBR® Green dye is a fluorescent dye that binds selectively to double-stranded DNA. The fluorescence intensity of the sample increases as soon as the number of double-stranded DNA increases.

There are several components in a fluorescence detection module. These are appropriate optical components such as lenses, dichroic mirror, emission filter and excitation filter as well as a light source and a detector. The fluorescence detection system has a similar configuration as a fluorescence microscope in which a light beam is

filtered by an excitation filter, reflected off by a dichroic mirror, hits the sample, goes through the dichroic mirror, filtered by emission filter and finally reaches to a detector. There are several options for light source and detector in real-time PCR systems. Regarding the light sources, xenon lamp, mercury lamp, tungsten lamp, LED and laser are the options. However, all the lamps and laser sources are usually expensive and bulky. LEDs are very cheap and small in size and used by researchers.[32,60] Laser diodes can be put into a category in between LED and other sources in terms of bulkiness since they rely on external power sources. On the detection side, charged couple device (CCD) image sensor connected to a microscope is used widely.[58,20] The data collected by the CCD is imaged to a computer screen. However, inclusion of a fluorescence microscope increases the footprint of the system greatly and makes it very hard to be a portable system. Another commonly used detector in PCR systems is photomultiplier tube (PMT). A PMT is a highly sensitive detector offering a high gain. Traditionally, these devices were big in size but today it is possible to find a small PMT (2.2 x 2.2 x 5 cm). Unlike a CCD, PMT gives a certain voltage and current output that does not require a screen to observe the output. Photodiodes and spectrophotometers can also be included in a PCR system as a detector.

1.3.7. Applications of Microchip PCR Systems

1.3.7.1. Human Diagnosis

PCR microfluidic systems have been employed in a wide range of DNA targets for human diagnosis. Researchers have shown the diagnosis of E. coli,[28,61,62] human

immune deficiency (HIV) virus,[50,63] human papillomavirus (HPV),[32] hepatitis virus,[64,65] Salmonella typhimurium,[29] M. tuberculosis,[38] malaria,[19] hereditary sideroblastic anemia,[26] B. anthracis,[66] hereditary hemochromatosis,[67] cystic fibrosis transmembrance conductance regulator (CFTR) gene[39] and Enterococcus faecalis.[68]

1.3.7.2. Animal Diagnosis

Some of the target DNAs for human can also be used to diagnose animal diseases however, most of the published works in the literature are proof-of-concept devices and they were not evaluated in clinics. One of the exceptions to that is the work of Cho et. al.[69] where they assessed the quality of the system for hepatitis B virus detection in humans. Animal specific PCR systems were not developed widely by researchers. One system to detect Maloney murine leukemia virus which causes cancer in mouse hosts was published by Obeid et al.[33]

1.3.7.3. Plant Diagnosis

The plant diagnosticians do not enjoy the microchip PCR systems as much as human diagnosticians since the microfluidic PCR chip systems developed for plant pathogen detection is very limited. Recently, one group demonstrated the detection of Phytophthora species which are fungal-like microorganism that cause Sudden Oak Death in North America.[70]

CHAPTER II

MICROCHIP PCR SYSTEM

2.1 Design and Simulation of Heaters

PCR is a very temperature sensitive protocol and ensuring accurate and uniform temperature distribution is essential for a successful PCR run. Having higher or lower temperature settings can result in no amplification or unspecific binding called as smearing. In order to have a uniform temperature over the chamber area, a square spiral heater that is similar to Kim et. al, [71] was designed. The heater was designed to be located on a 25.4 x 25.4 mm glass chip. The gap between the legs of the spiral design is 630 μm and the width of the outermost leg is 1280 μm. The widths of the legs get bigger by a ratio of 1.25 in succeeding leg and the widest leg is placed in the middle of the chamber. The legs have widths of 1600, 2000 and 2500 μm. The design was drawn and simulated in COMSOL Multiphysics® software (A detailed manual for the software can be found in Appendix A). In the simulation, a PCR chamber having a circular shape in 7.8 mm diameter with inlet and outlet in sizes of 4.4 x 2.7 mm located in a 25.4 x 25.4 mm glass slide and etched to a depth of 80 μm was also included in the simulation. The 80 μm gap was filled with water in the software. The thicknesses of the both glass slides are 500 μm. The metal used in the heater is chosen to be gold and time-dependent simulations are done while applying positive voltage and ground from the edges of the heater. It takes around 17.5 seconds for the water inside the chamber to reach around 95°C. Once the time reaches 17.5 seconds, the software stops and the temperature

distribution can be observed. The top view cut from the middle of the chamber and cross-sectional view cut from the center of the chamber are shown in Fig. 2.1. As can be seen from the top view and cross section views, the temperature inside the chamber is within 2 degrees.

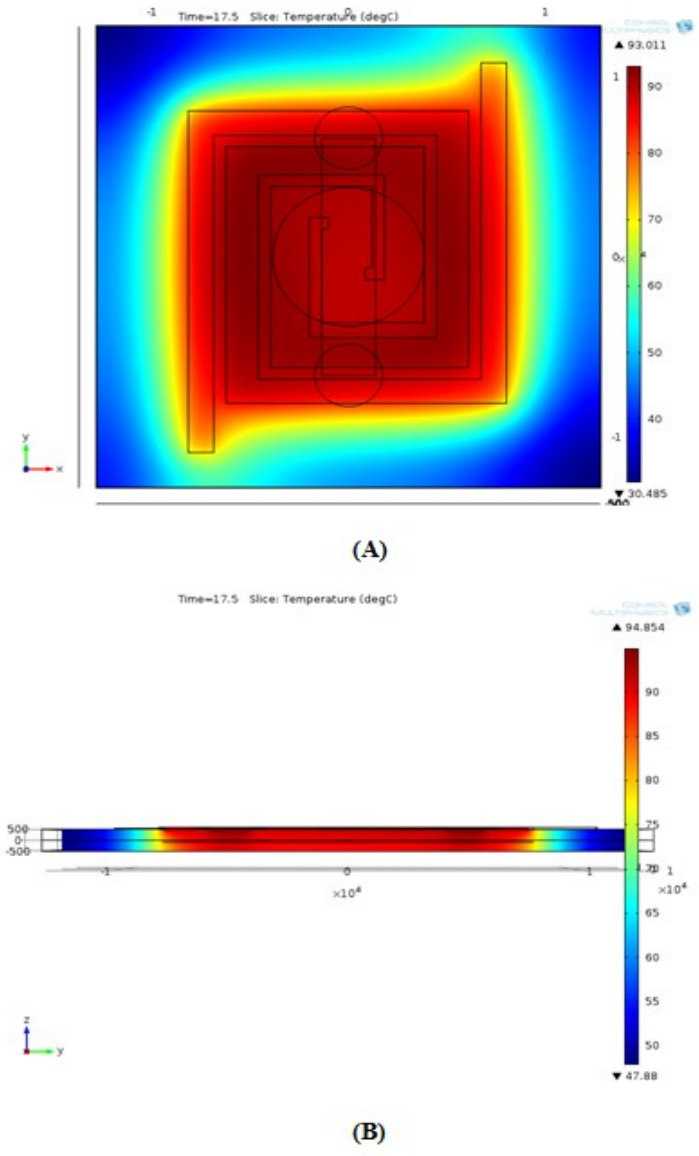

Fig. 2.1 Top view (A) and cross-section (B) of the square spiral design

2.2 Microfabrication of Devices

The microchip device was fabricated using standard photolithography and etching. For the microchamber part, after cleaning the borofloat glass with piranha solution (H_2SO_4:H_2O_2 = 3:1 (v/v)) for 20 minutes, the glass slide was rinsed and dried. Chromium and gold deposition using e-beam evaporator was done. Following the deposition, photoresist (Microposit® S1818, Rohm-Haas-Shipley Company, Inc., Marlborough, MA, USA) was spin-coated onto the wafer at 4000 rpm for 30 sec with an acceleration of 5. Afterwards, the glass was soft baked for 4 minutes on 110°C hot plate. The glass was loaded into mask aligner (Karl Suss MA6 Mask Aligner, SUSS Microtec, Inc., Waterbury Center, VT, USA) and exposed to UV light for a dosage of 87 mJ/cm^2. Following the exposure, the glass was developed using developer (Microposit® MF-319, Rohm-Haas14 Shipley Company, Inc., Marlborough, MA, USA) for around 1 minute. The metal layer on the glass slide was selectively etched using Au and Cr etchant. The back side of the glass was taped using optical adhesive tape (MicroAmp® Optical Adhesive Covers, Applied Biosystems, Beverly, MA, USA) to avoid etching of the back side. Next, hydrofluoric acid (HF) solution was prepared ((49%HF (J.T. Baker):H_2O = 5:1 (v/v))) and the glass slide was immersed into the solution for around 19 minutes to achieve a depth of 80 μm. During the glass etching, the solution was agitated to have a uniform etching. After the HF etching, the glass slide was rinsed for 20 minutes and the remaining metal was etched using Cr and Au developer. Since there are four patterns in one glass slide the glass slide was cut into four using Professional Laser Series (PLS) 6.120D Laser Engraving and Cutting System (Universal Laser Systems, Inc., Scottsdale,

AZ, USA) using 50% power and 10% speed. Before drilling the inlet and outlet holes, wax CristalBond^{TM} 509 (West Chester, PA, USA) was applied to avoid cracks on the glass during drilling. After the drilling, the wax was removed using acetone. For the heater part, same procedure was applied up to HF etching part and the heater was ready to use. The microchamber and the heater was bonded together using UV glue (Loctite 3492, Dusseldorf, Germany) and cured under UV light curing system (OmniCure S1000, Lumen Dynamics, Mississauga, Ontario, Canada) for 5 minutes. A fabricated device is shown in Fig 2.2. The overall fabrication procedure is summarized step by step in Fig.2.3.

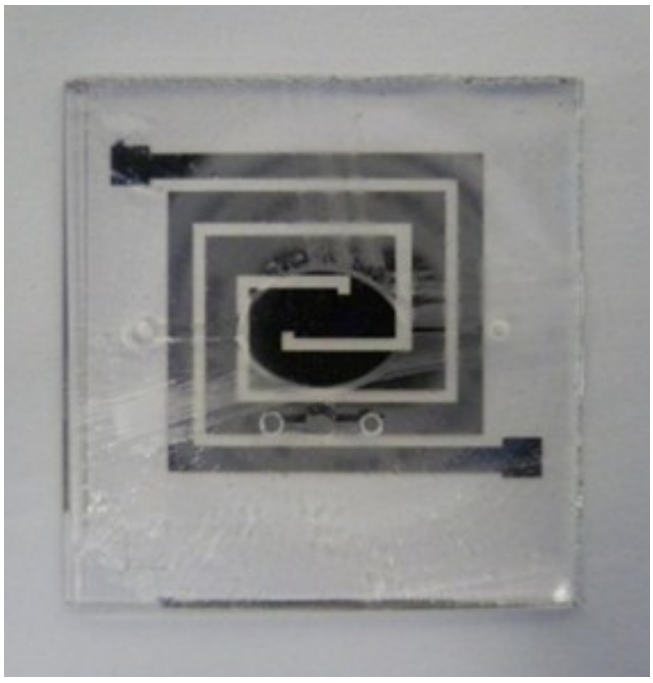

Fig 2.2 A picture of a PCR microchip having a chamber and heater bonded with a UV glue

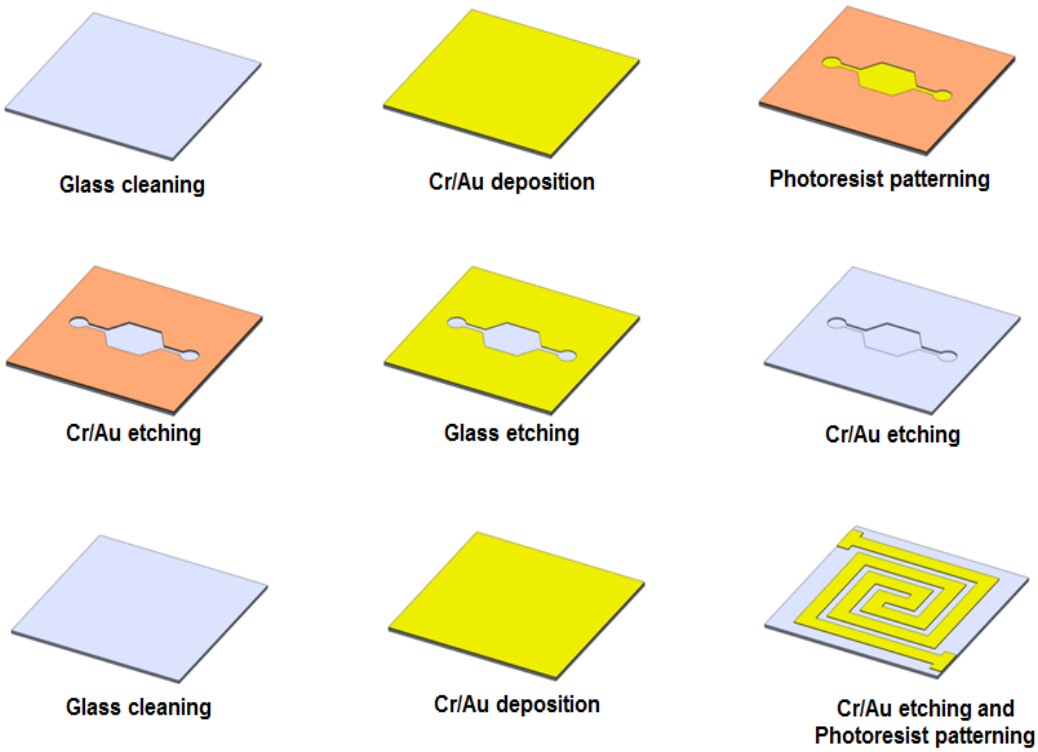

Fig 2.3 Microfabrication procedures

2.3 Temperature Characterization of Heaters

2.3.1 PID Control of Heaters

In order to have an effective PCR result, it is mandatory to have correct settings of temperature zones and duration. However, while heating up the sample some undesired characteristics of the heater such as overshooting and undershooting might be observed when there is no specific controlling method is in effect. The switching on and off the heater without a feedback control can cause overshoot and affect the performance of the PCR experiment. This is where controlling methods are desired. One such

method is proportional-integral-derivative (PID) control which is a method to keep variables of a system within a desired range. The feedback idea lies at the core of the PID controller and is a powerful method.[72] The PID controller is the most widely used controller method in all controlling systems in many industries to solve problems in process control, motor drives, automotive and flight control. The integral, proportional and derivative feedback is based on past (I), present (P) and future (D) error. The proportional term defines the sensitivity of the system where a small P value can make the system insensitive to changes but a big P value can cause the system become unstable and provides an overall control.[73] The integral term defines the speed of the movement of the system to a desired value where the bigger the I value the faster the system will be but a big I value can cause overshooting and reduces the steady state error. Lastly, the derivative term increases transient response meaning an increased D value can result in increased stability of the system. A general PID control system schematic is shown in Fig 2.4 and illustrates the feedback control of the system.

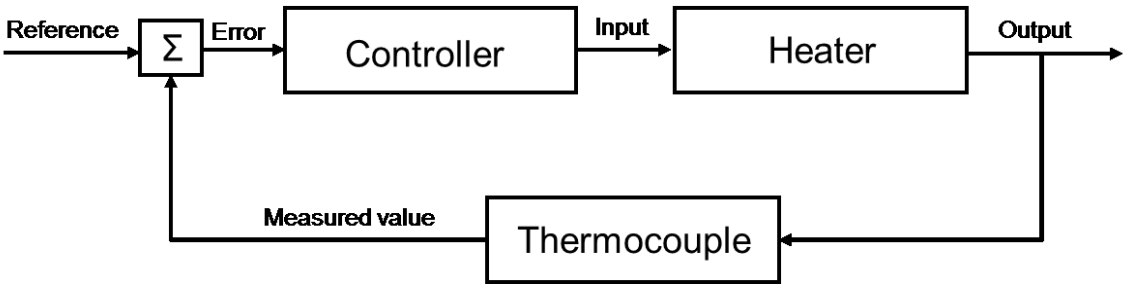

Fig 2.4 General working principle of PID control. The feedback is sent back to the system for reliable control

2.3.2 Temperature Profile of the Devices

The temperature profile of the heater was measured using K type thermocouples (Omega Engineering, Stamford, CT, USA) that is connected to a thermocouple input National Instrument Module NI 9211 (Austin, TX, USA). Firstly, the thermocouple is calibrated using boiling water in a beaker. The temperature settings are compensated for the difference.

The temperature setting for an efficient thermocycling is determined by placing a thermocouple on top of the heater corresponding to the middle of the chamber and another thermocouple to the reference point at the back of the device. An illustration of the temperature calibration setting is shown in Fig. 2.5. The difference of two thermocouple locations gives ideal temperature settings for the PCR experiments since it has been determined before that the temperature difference between the top of a glass slide and bottom of it gives around 0.3°C difference and the temperature at the top of the heater is very close to the temperature of the top of the sample.

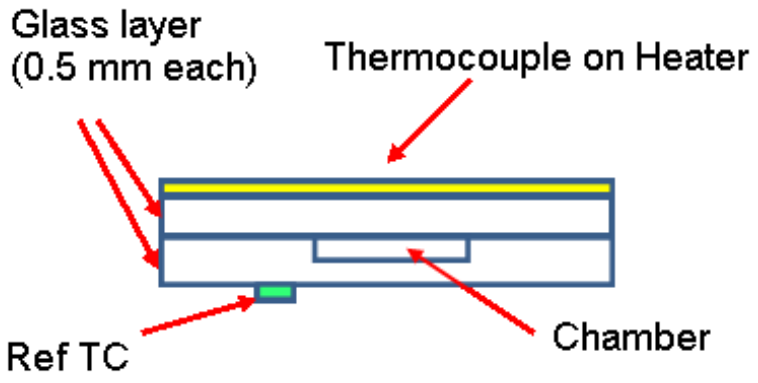

Fig. 2.5 Schematic used to determine temperature settings. Two thermocouples placed on different sides of the device

The calibration test was done and is shown in Fig. 2.6. According to the experiment, the temperature difference is found out to be 11°C for denaturation zone, 8°C for extension and 6°C for annealing zone. The settings for PCR experiment in this case is 84°C for hot-start, 83°C for denaturation, 64°C for extension and 55.5°C for annealing temperature.

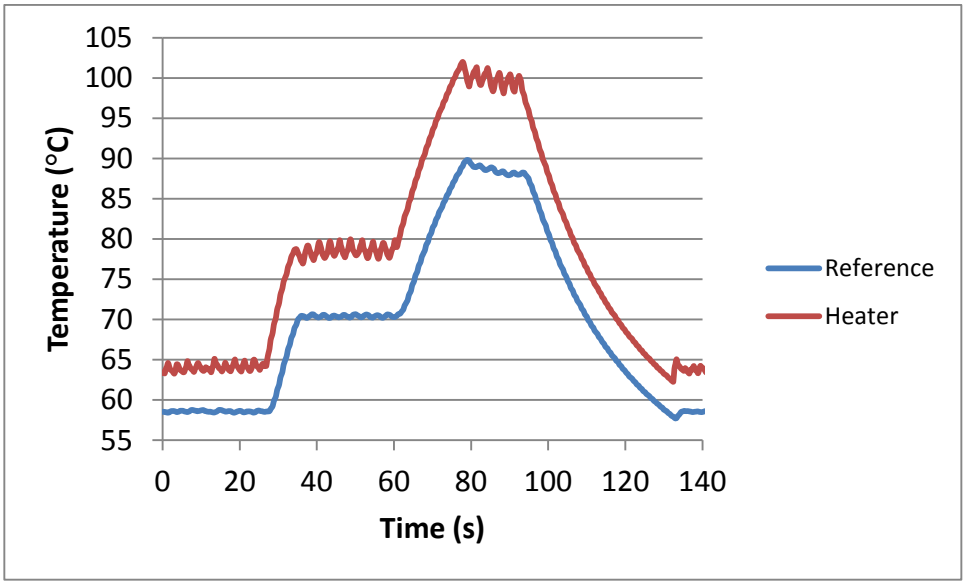

Fig. 2.6 The temperature profile from the two thermocouples placed on different sides of the device

After finding out the temperature settings, a full PCR run using PID parameters of 8000, 0.05 and 0.001 for hot-start, denaturation and annealing temperature zones and 8000, 0.2 and 0.05 for denaturation zone. The full 35 cycle run is shown in Fig. 2.7. As can be seen from the figure, the overshoot is limited to about 1°C and no undershooting was observed. Another important parameter in thermocycling is to achieve same profile in each PCR cycle and this criterion is also satisfied by the PID controller.

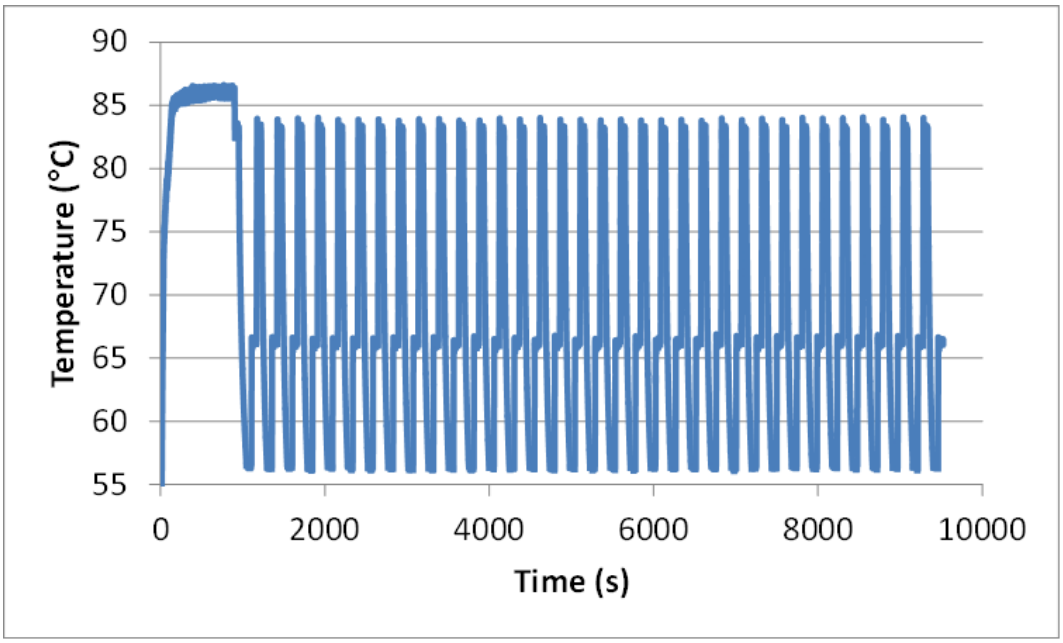

Fig. 2.7 Full run of PCR cycle demonstrating repeatable temperature profile in each cycle

2.4 Optical System Design and Characterization

2.4.1 Overview of the Optical System

The optical system for PCR product detection is based on fluorescence microscopy idea where the sample is illuminated with light and different color light having longer wavelength coming out from the sample is detected. The components of the fluorescence detection system consists of a light source to illuminate the sample, an excitation filter to block the undesired range, a dichroic mirror that reflects the excitation wavelength range but passes the emission wavelength range and lastly an emission filter to make sure none of the excitation light goes in to the detector. Additionally, lenses are used to focus the light and mirrors are used to reflect the light to detector.

In this work, SYBR Green dye is present in the PCR buffer and has a peak excitation of 497 nm and peak emission of 520 nm. A blue LED NSPB310B (Nichia, Tokushima, Japan) which has a dominant wavelength of 470 nm is used. To illuminate the blue LED under constant current, LM317 integrated circuit (National Semiconductor, Santa Clara, CA) is used with 180Ω resistor to have current of 7 mA. The excitation filter used is ET470/40x (Chroma Technologies, Brattleboro, VT) which passes the light between 450 and 490 nm only. After the excitation filter, the light is focused with a lens having 14.9 mm focal length and 12.7 mm diameter (ThorLabs, Newton, NJ) and hits a dichroic mirror that lies 45° to the ground (495dclp, Chroma Technologies) which reflects the blue light upwards to hit the sample. Before hitting the sample, the light passes through an aspheric lens (ThorLabs) which is 6.7 mm in diameter with a 0.68 numerical aperture (NA) and has a working distance of 1.76 mm. As soon as the light hits the sample, fluorescence emission takes place and will pass through the aspheric lens and goes towards dichroic mirror. The dichroic mirror will reflect the blue light while passing the green light. The green light hits a silver mirror that has a 25.4 mm diameter. Finally, the light is filtered with an emission filter (ET535/50m, Chroma Technologies) to block all the light that has less than 510 nm wavelength. The light is sensed by a photomultiplier tube (PMT) that is located at the end of the optical system. The PMT employed in the experiment is 931A (Hamamatsu, Hamamatsu City, Japan).

The optical housing for detection of PCR samples illustrating the trajectory of the blue and green light is shown in Fig. 2.8.

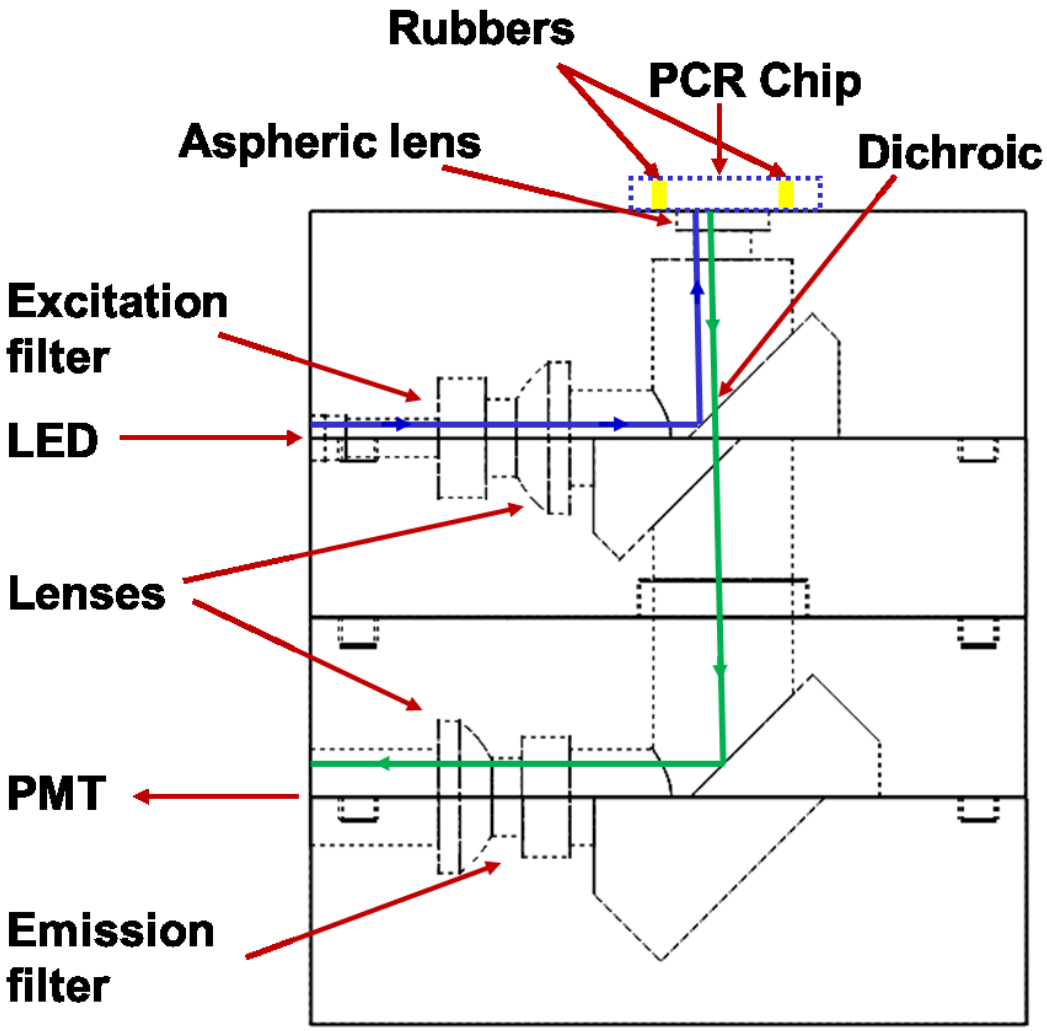

Fig. 2.8 The optical housing schematic used in fluorescence measurement. The blue ray is the trajectory of the LED and the green ray is the trajectory of the fluorescent light coming from the sample

2.4.2 Optical Housing Production and Microdevice Integration

To hold the optical components, an optical housing is made using 3D printer (envisionTEC Ultra, Marl, Germany). The appropriate scheme was drawn in SolidWorks software (Dassault Systems, Waltham, MA), modified in 3D printer

software to generate appropriate image files and transferred to the machine. 3D printer has a light sensitive resin and selectively reflects the light just like a projector and light solidifies the resin. The stage moves up and a new image file is loaded to 3D printer. In this fashion, truly 3D structures can be produced in layer-by-layer fashion. The overall size of the optical housing is 3.9 x 5.9 x 11.9 mm. All the parts reside inside the housing except for the PMT which is tightly attached to the housing. The fabricated optical housing with the structures is shown in Fig. 2.9.

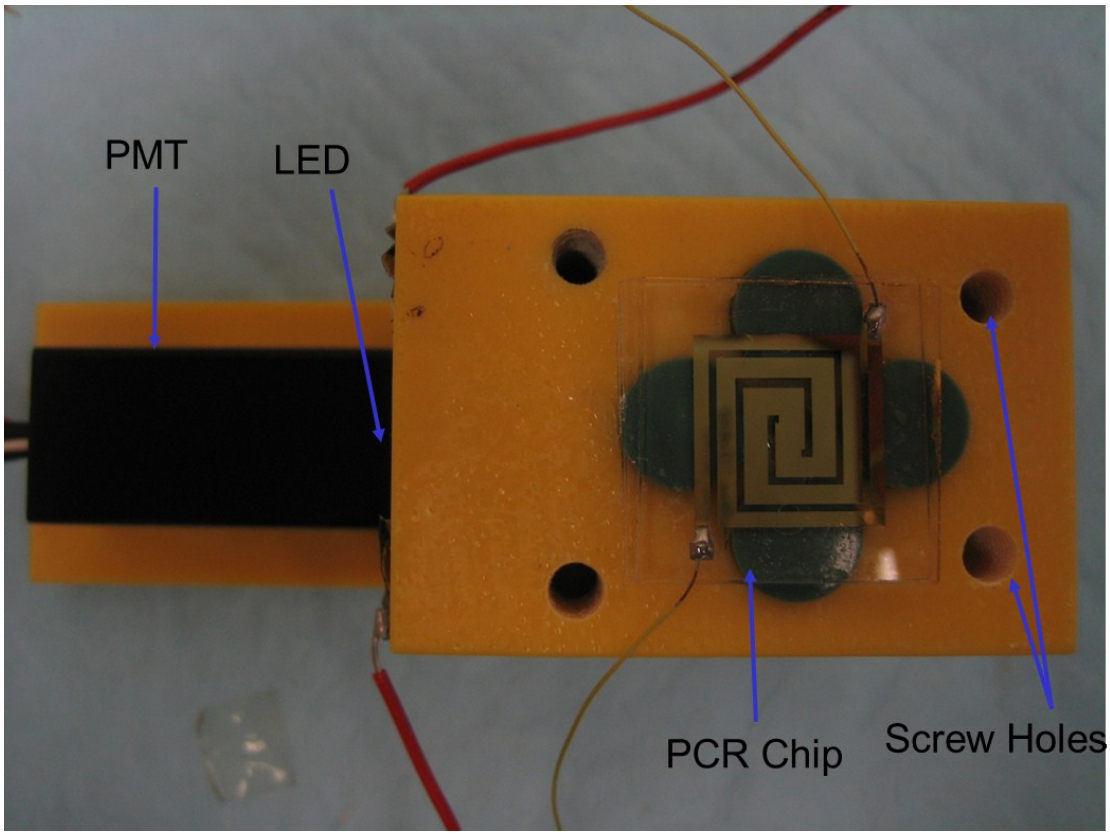

Fig. 2.9 Manufactured optical housing using 3D printer. The LED is placed inside the housing and green septa rubbers are used to seal the inlet and outlet of the microdevice

The integration of the PCR chip is accomplished by using gastight rubbers (ThermoGreen^{TM} LB-2, Sigma-Aldrich, St. Louis, MO) on both sides of the microdevice. After placing a cover layer with rubbers, screws are used to ensure a tight sealing and avoid evaporation of the sample.

2.4.3 Optical Characterization of the System

The efficiency of the optical housing is tested using a spectrophotometer to ensure appropriate excitation of the sample and reliable reading from the detector location. Three different conditions are tested: LED's wavelength, the excitation filter output while the LED is on and reading from the detector location part of the optical housing. The relative intensities of the three conditions are shown (Fig. 2.10).

According to the spectrophotometer results, the LED has some 500 nm or more wavelengths which might affect the fluorescence efficiency but it is efficiently blocked by the excitation filter. Finally, the reading from the detector part reveals that only fluorescence part is detected by the detector and no blue light is present in that location.

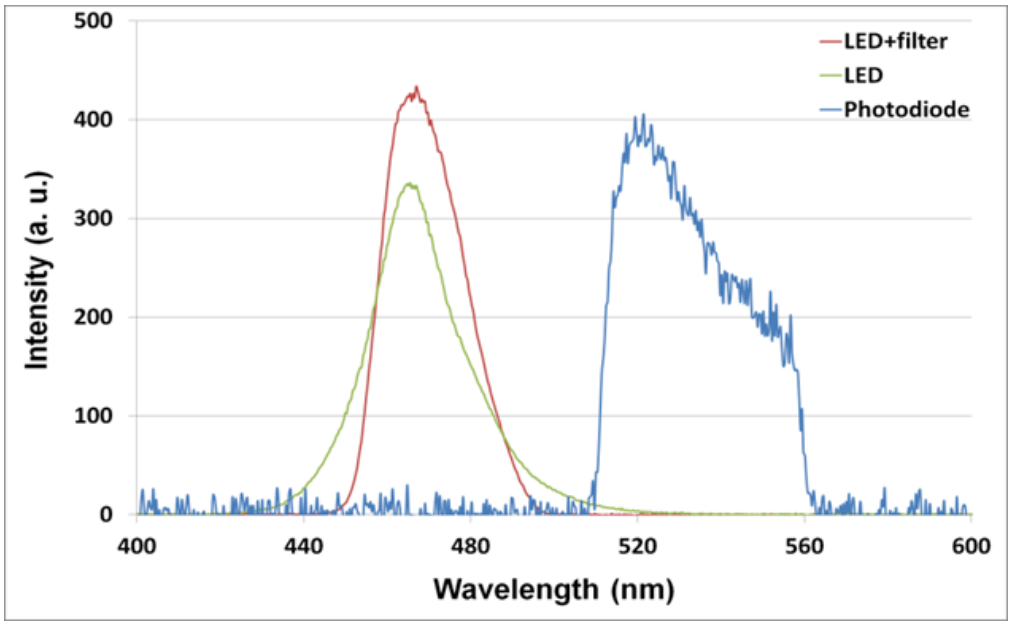

Fig. 2.10 Spectrophotometer results showing suitable excitation and emission optical components. The excitation filter blocks out the green light coming from the LED and only green light range is observed from the output

2.4.4 Characterization of Fluorescence Detection Capability of the System

The optical system has been characterized in two ways. Firstly, a test involving concentrations of Fluorescein isothiocyanate (FITC) ranging from 0 nM (DI water) to 2500 nM was done. For this purpose, an etched chamber layer is bonded to a plain glass of same size and small (2 x 2 mm) Polydimethylsiloxane (PDMS) slabs including holes were bonded on top of the inlet and outlet using plasma treatment. Tubing was attached to inlet and outlet parts of the microdevice and desired concentration was injected into the device using a syringe. Second characterization was done using PCR samples to observe the difference between amplified and unamplified samples. Unamplified sample was mixed and measured using the same fashion and amplified sample was conventionally amplified using thermocycler before measurement. The graph for both experiments is shown in Fig. 2.11.

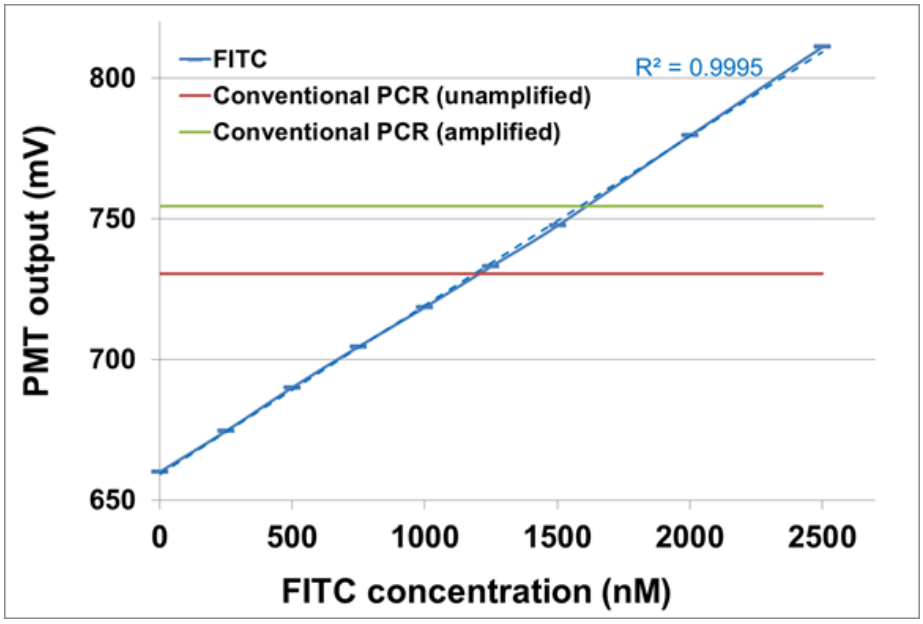

Fig. 2.11 PMT characterization using fluorescent dye and PCR samples. Linear increase in PMT output was observed for different dye concentrations. Additionally, unamplified and amplified sample resulted in different PMT outputs making it suitable for PCR experiments

As seen in the graph, the FITC concentrations gave a linear increase throughout the experiment. Additionally, there was a 25 mV increase from unamplified to amplified sample. Based on these finding, the optical system is considered to be efficient for PCR experiments.

2.5 Developments towards a Multi Chamber Microchip PCR Design

After having achieved a heater design capable of generating a uniform temperature distribution which is a good candidate for PCR experiments, additional heater designs were considered for smaller chamber dimensions. The aim was to squeeze three or four heaters in a 25.4 x 25.4 mm glass slide instead of one. The

chamber size becomes 3.5 x 6.5 mm. Several designs that are capable of heating the sample inside the chambers were made and tested.

Firstly, the square spiral design was tested after reducing the size of the design and connecting the four square spiral designs by a straight channel. The resulting temperatures inside individual chambers are within several degrees however, there are significant temperature differences between the temperatures of different chambers.

To overcome this problem, unconnected heater designs were considered. One design has four bar shape heaters to heat four small size chambers. The heaters are in 21 x 5 mm with additional pads for soldering. Voltage is applied from pads and to all of the heaters, which is running four heaters at the same time. A uniform temperature distribution was observed around where the chamber would be located and is shown in Fig. 2.12. The chambers in the middle and the chambers at the edges have the same temperature range that differs from the other group.

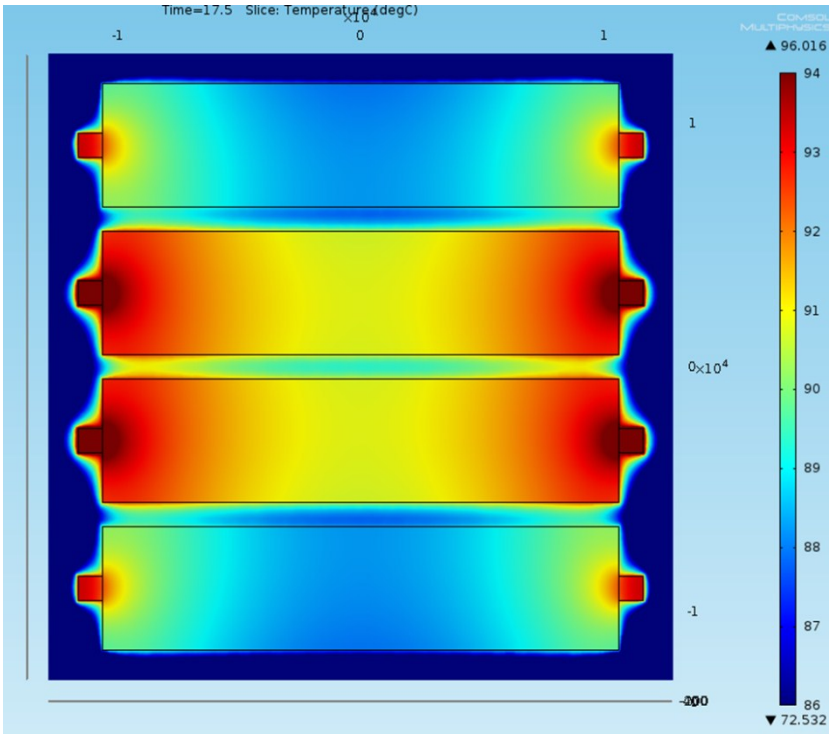

Fig. 2.12 Simulation result of 4-bar design. Similar profile was observed from middle chambers and edge chambers but the two groups have different temperature profile

However, an issue of this design is that the heaters have a low resistance. When fabricated, it is observed that one heater draws around 1 Ampere at 2 Volts and running even two heaters at the same time would require 2 Amperes which is a substantial increase compared to the single chamber design where the drawn current is less than 0.5 Ampere. Based on this finding, simulations running one heater at a time were done and found out especially the edge chambers have a non-uniform temperature distribution and avoid successful PCR runs. The edge chamber simulation is shown in Fig.2.13.

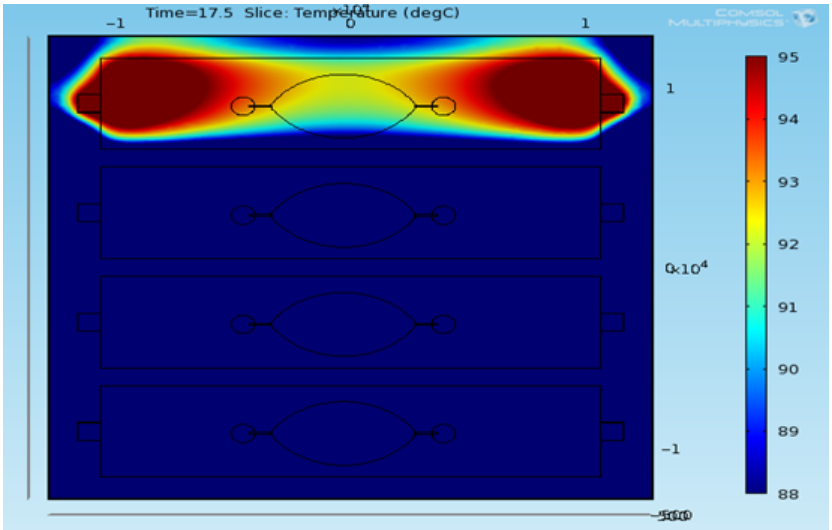

Fig. 2.13 Simulation of one chamber in 4-bar design. The temperature difference within the chamber is up to 5 degrees

Another issue with the four design heater is the reference point where the thermocouple is located is very sensitive to temperature distribution if the reference point is placed at the back side of the device slightly off the chamber to avoid spanning the optical reading area. It can also be seen on the simulation result that the temperature drops fast on the corners of the chamber (Fig.2.13). Moving the thermocouple by several millimeters changes the temperature difference between the top of heater and reference point significantly. Temperature profile of the individual four-bar heater was done the same way as before, that is placing one thermocouple on top of the heater and the other thermocouple on the back side on a reference point that is slightly off the chamber. The temperature profile is shown in Fig. 2.14 and the temperature differences between two points are 14°C for denaturation, 8°C for extension and 4°C for annealing temperature. However, the temperature differences varied from experiment to

experiment because of placing the reference thermocouple slightly closer or to farther from the chamber.

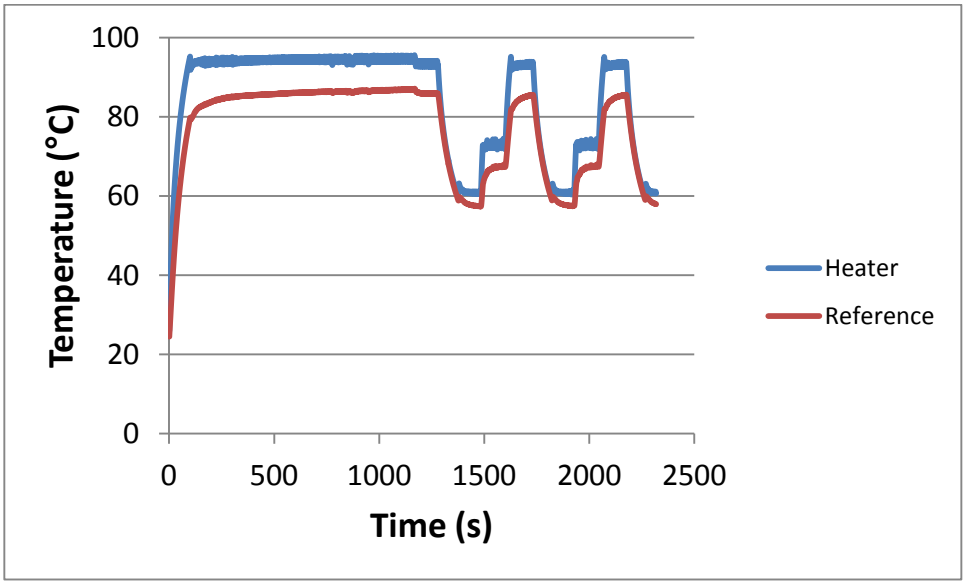

Fig. 2.14 Temperature profile of the 4-bar design. The difference between two thermocouples is significant and since the reference thermocouple is very sensitive to location there is a run to run variance in this experiment

The problems with the four-bar heater design led to seek for a better design that has a better temperature uniformity when running individual chambers. So, a design to have a higher resistance was designed which is a serpentine shape design that covers the area of individual chambers. The serpentine heater is 19.4 x 5 mm in size while each leg of the heater is 500 µm thick and the gap of each leg is 200 µm. Both middle chamber and edge chambers were simulated while the water is introduced in the chamber. The middle chamber temperature is within 2 degrees and good uniformity is observed. On the other hand, the edge chamber temperature while within several degrees has a slightly

shifted temperature gradient but it is considered as good enough for PCR thermocycling. The simulation of both cases is shown in Fig. 2.15.

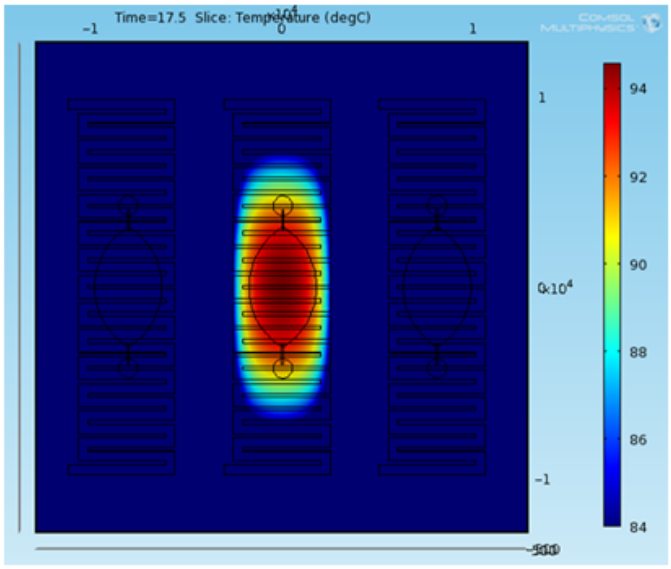

(A)

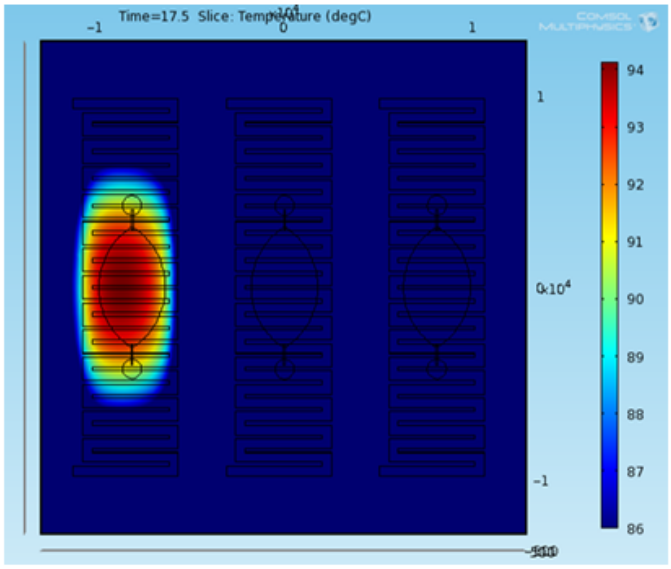

(B)

Fig. 2.15 Temperature simulations of serpentine design. Top views of (A) middle and (B) edge chamber are shown. The temperature inside the chamber is within 2 degrees

Observing good uniformity in simulations of the serpentine design, it was fabricated (Fig. 2.16) and temperature profile was tested using two thermocouples attached on top of the heater and at the back side of the heater after fabricating the microdevices. The main reason to change the position of the reference point is to avoid having a big temperature difference by slightly moving the thermocouple. The temperature profile is shown in Fig. 2.17 and the temperature differences between two thermocouples are 4.5°C for denaturation, 2.5° for extension and 1.5° for annealing temperature. The experiment was repeated several more times and low experiment to experiment variation was observed.

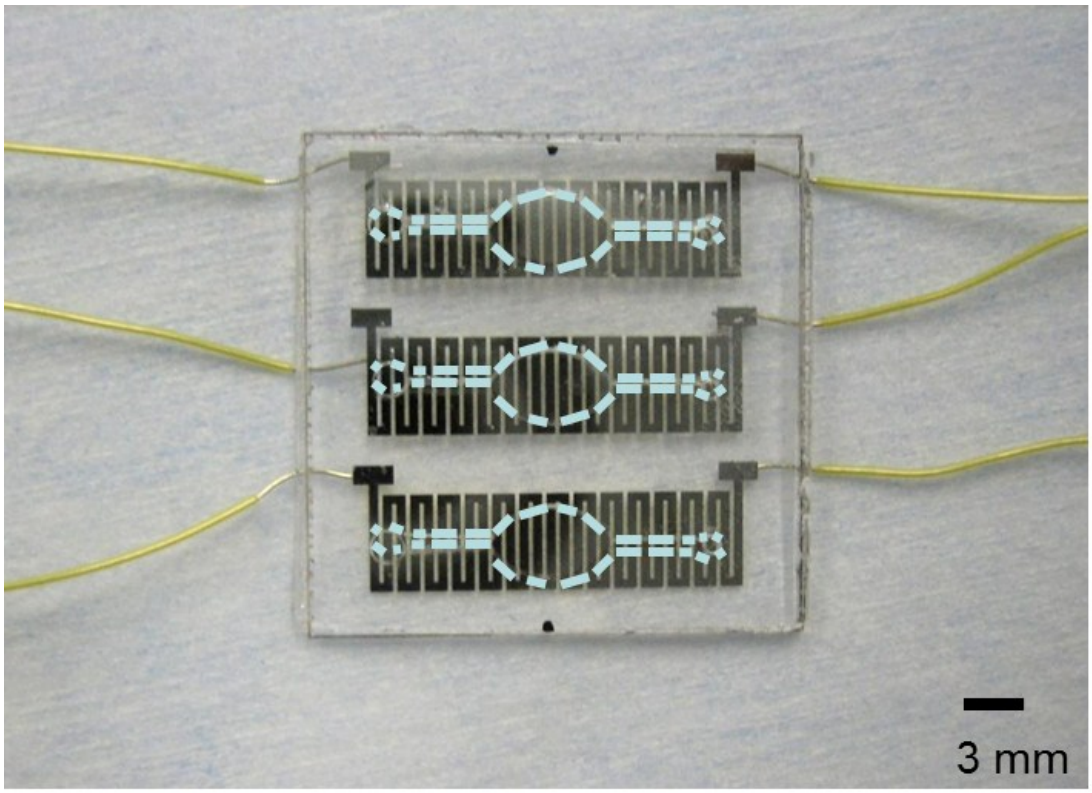

Fig. 2.16 Fabricated serpentine design microdevice

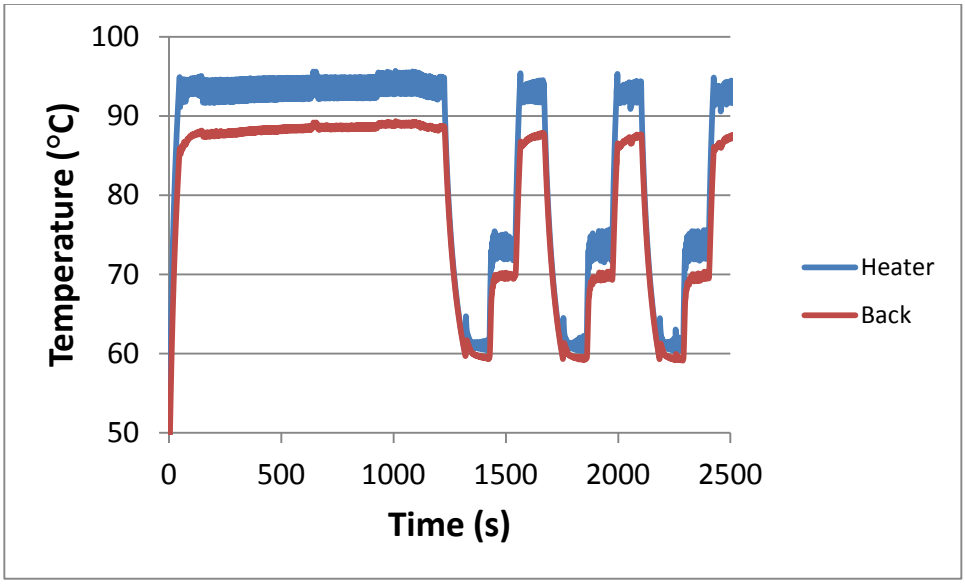

Fig. 2.17 Temperature profile of the serpentine design. There is a small difference between two thermocouples and the variance from run to run is small

The serpentine design gave a better performance in terms of drawn current (0.2 A) and temperature uniformity and it was decided to use serpentine design for multiple chamber microdevices. The thermocouple was decided to be placed on top of the heater during the PCR thermocycling and the set temperatures are determined to be 96.5°C for hot-start, 95.5°C for denaturation, 73°C for extension and 61°C for annealing temperature.

CHAPTER III

DEVELOPMENT OF THE PORTABLE PATHOGEN DETECTION LAB ON A CHIP (PADLOC)

3.1 Overview of the PADLOC System

The PADLOC system is composed of three subsystems. These are microfabricated PCR chip with integrated heater, a fluorescence detection system and a controller system. The thermocycling of the sample is done by the heater on the PCR chip while controlled by a controller system that is hooked up to a computer and thermocouple is used as a temperature sensor. The controller system also arranges the timing of light source and recording of optical detector. The overall structure of the PADLOC system is shown in Fig. 3.1.

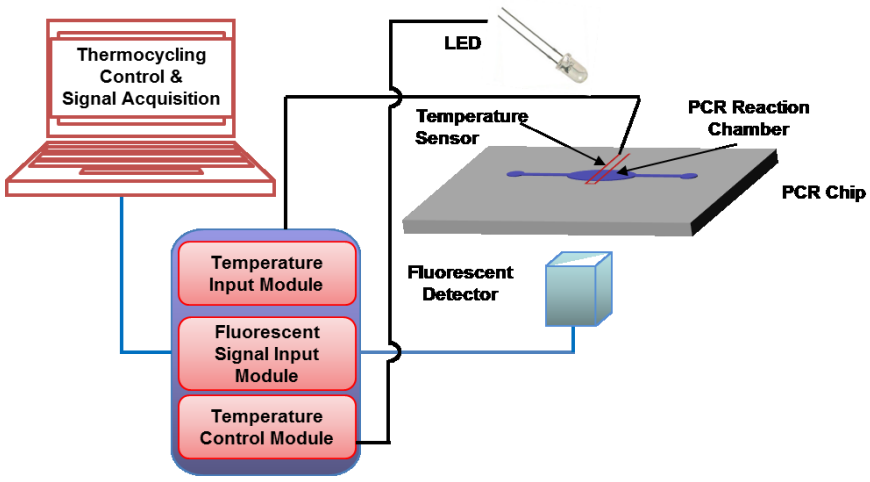

Fig. 3.1 Overall view of PADLOC system having microdevice, optical setup and control and acquisition modules

3.2 System Control and Operation

The control of thermocycling and optical excitation and detection is done using NI LabVIEW software. LabVIEW is the software of choice when working on data acquisition. With additional hardware modules, it is possible to read, write, manipulate and output physical quantities such as voltage, current, resistor, temperature, stress, strain, etc. A general outline of the LabVIEW software used in PADLOC system is shown in Fig. 3.2.

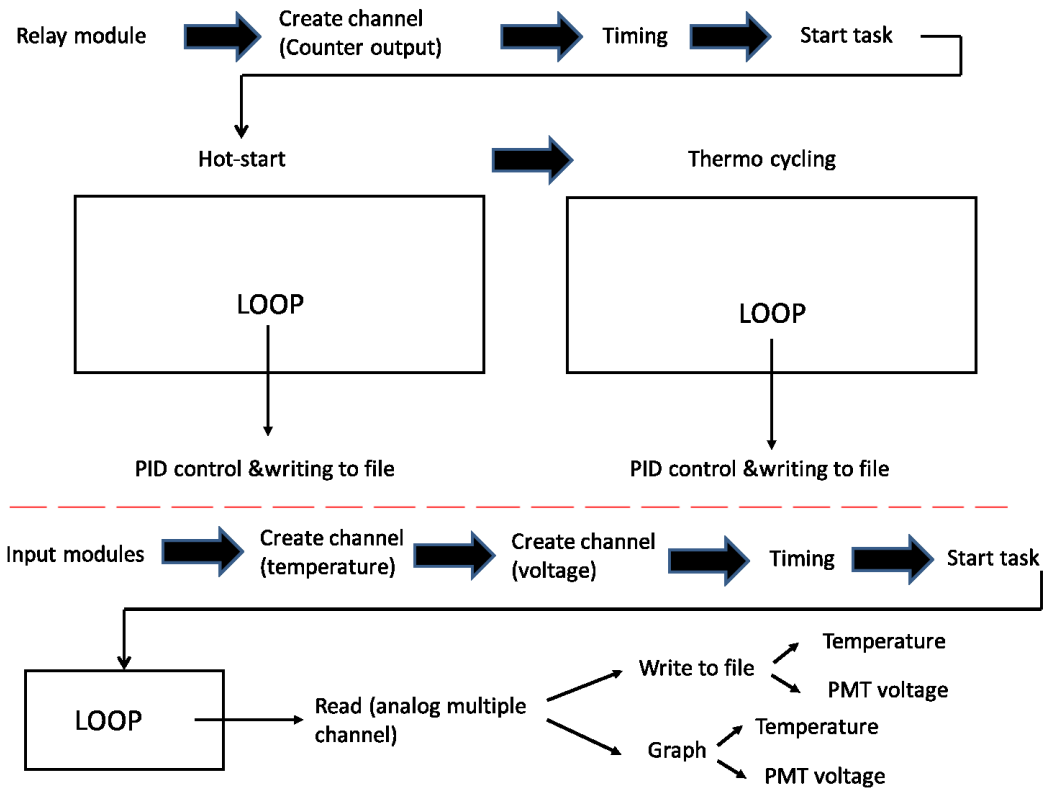

Fig. 3.2 The structure of the Labview program for PCR experiments. It can be regarded as a combination of two programs: One for temperature control and one for data acquisition and display

Three different NI modules are used in the system. These are NI 9481 which is a relay module that transmits or rejects the supplied voltage according to control parameters, NI 9211 which is a thermocouple input module to sense the temperature of the sample and NI 9205 module which is a voltage input module used to read PMT voltage. All these modules are located on a NI 9172 chassis. The relay module is used to control the thermocycling of the PCR chip as well as to turn on the LED on the last second of extension temperature zone. The PMT input voltage is read differentially meaning that two cables are connected to the voltage input module and it reads the difference of the two wires. The wires are coming from positive and negative output of the PMT.

The software first initializes the relay module and creates a counter that controls the timing of the PCR experiment. After creating a counter and a virtual channel, hot-start part of the experiment starts. The software goes into a loop of heating the sample to hot-start temperature until the specified time (in our experiments it is 15 minutes) is over. While the program is in the loop it also executes PID control using the internal PID functions of NI LabVIEW PID and Fuzzy Logic Toolkit add-on. Following hot-start, the software executes thermocycling of denaturation, annealing and extension temperature zones in a loop similar to hot-start. The three temperature zones are alternated until the desired cycle (usually 35 cycles in our experiments) is completed and relay module turns on the LED on the last second of the extension zone for each cycle. While the relay module accomplishes the thermocycling and LED excitation based on the software, the voltage and temperature input modules create channels for temperature

and voltage in a similar fashion. The input tasks are started at the same time as relay module. The temperature input is read continuously during the PCR experiment in a loop and the temperature data is written to a file. The voltage input is read for only one second in each cycle since the LED illuminates the sample in that specific second in order to avoid photobleaching of the PCR sample. The voltage data is also written to a separate file. The temperature and PMT output is also displayed on the PC screen on the front-end of the LabVIEW program. The front-end includes selection of temperature durations, cycle times and file selection for temperature and voltage data as well as graphs for temperature and voltage data. The front-end of the LabVIEW program is shown in Fig. 3.3.

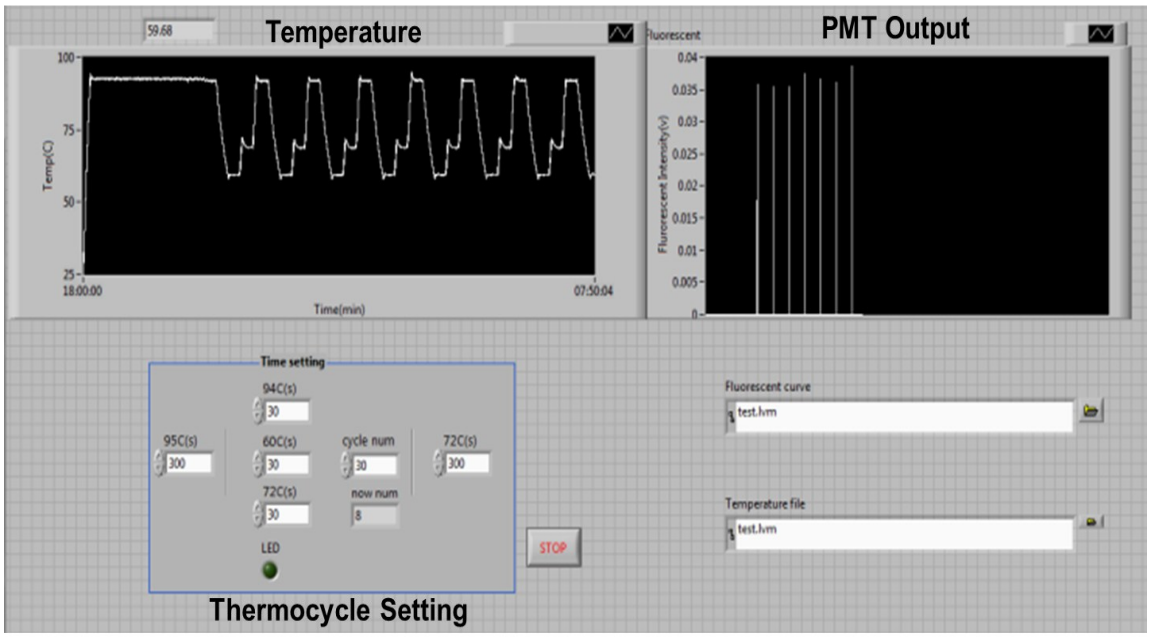

Fig. 3.3 Front-end of the Labview program. It allows entering temperature durations and files to log the data as well as displays temperature and PMT output data

3.3 Specifications of the System

The PCR chips used in the experiments have 200 Å Cr and 1800 Å Au layer and they have around 30Ω resistance for square spiral design and 100Ω resistance for serpentine design. The applied voltages to the heaters are between 10 and 15 V.

On the optical detection side, a constant current source integrated circuit (IC) is used to ensure same light excitation intensity in every cycle. An 180Ω resistor is connected in between the IC's legs to have a current of 7 mA. The LabVIEW software is set to read 14 samples per second which is the maximum limit for temperature input module. The PMT is powered to 14.3 V using a power supply (mastech, Pittsburg, PA). In the voltage measurement file, 14 samples are output for each cycle since the voltage is read for only one second when LED is on. The first five values for each cycle are discarded since the LED intensity doesn't reach its full brightness right after it is on and results in low output reading. The remaining samples are averaged using Microsoft Excel software and the voltage increase is plotted against cycle number.

The size of the optical housing is 3.9 x 5.9 x 11.9 mm including the PMT and the overall size of the NI modules are 250 x 85 x 90 mm. Additionally, a small part of a breadboard is used for constant current source circuitry, power supplies for heater, LED and PMT. Lastly, a computer is used to run LabVIEW software. The system itself without computer and power supplies uses small space and is portable.

PADLOC system performance is compared to a conventional thermocycler that can be found in plant pathology labs using the same pathogen and PCR kits. The heating

and cooling times of the thermocycler are included together but are given separately in our work. The table is shown in Table 3.1.

Table 3.1 PADLOC system and thermocycler temperature durations

	This work	Conventional Thermocycler
Hot-start	915 s	900 s
Denaturation	48.5s x 35 = 1697.5 s	15s x 35 = 525 s
Annealing	59s x 35 = 2065 s	30s x 35 = 1050 s
Extension	58s x 35 = 2030 s	30s x 35 = 1050 s
Warm up	557 s	2475 s
Cool down	2471 s	
Total	2 h 42 min	1 h 40 min

3.4 Sample and Reagents

Before starting the PCR experiment, both the rubbers and PCR microdevice are sterilized using autoclave in order to avoid any contamination problems. The devices are coated with Bovine Serum Albumin (BSA) having concentration 10 mg/ml for 15 minutes in order to avoid adsorption of the sample on the microdevice walls. Afterwards, the BSA inside the chamber is sucked and prepared sample is loaded inside the chamber.

The samples are stored at -20°C and they are thawed on ice before preparation. A 20 µl sample is prepared using 10 µl of Sybr Green PCR master mix (Qiagen, Valencia, CA), 5 µl RNase –free water, 1 µl forward and reverse primers having5'- TCG

TTT CCA GGA AAG CTG C -3' and 5'- GCA GCT TTC CTG GAA ACG A -3' , 1 µl 10% Polyvinylpyrrolidone (PVP) and 1 µl 1 mg/ml BSA. The sample in the tube was mixed using a vortex mixer for several seconds and injected into the BSA-treated chamber.

3.5 Detection of Pure Genomic DNA

3.5.1 Detection using PADLOC and Validation

PCR experiments were done using pure fungal genomic DNA to amplify part of SIX1 gene from Fusarium oxysporum spf. lycopersici. The total PCR experiment has a 15 minute hot-start following a 35 cycle of three temperature zones for 50, 60 and 60 seconds. After averaging the samples as described in specifications section, Excel plots are obtained and are shown in Fig.3.4.

According to the PMT output, an expected increase in PMT voltage was observed. The voltage profile of the experiment in the presence of target DNA showed an obvious increase in the fluorescence of the sample which was expected.

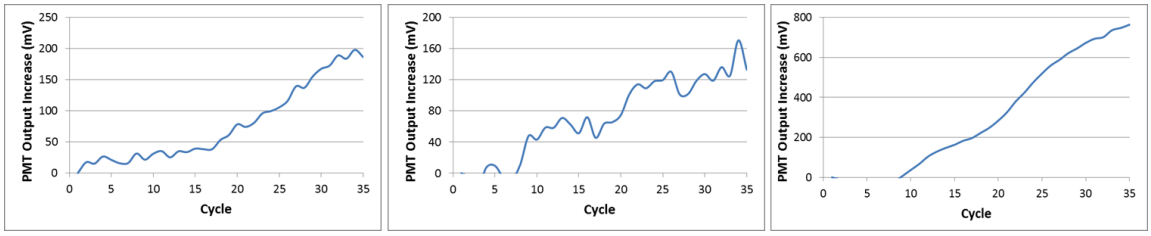

Fig. 3.4 PMT outputs of three PCR runs. The fluorescence intensity increases were shown

To verify the PCR amplification results, gel electrophoresis was also done after the experiment. The sample was extracted using a pipette and loaded in 1.2% agarose gel. After preparing the agarose in 0.5x TBE buffer and boiling in microwave oven for 50 seconds, the mixture was left for solidification. The gel was run in 0.5x TBE buffer at 95 V for around 50 minutes. For PCR ladder, 7 µl 1Kb PCR ranger (GenDEPOT, Barker, TX) was loaded in the first well. Before loading the sample, they are mixed with 6x loading dye (New England Biolabs, Ipswich, MA). Following the 50 minute voltage exposure, the gel was taken out of the buffer and the picture was taken as the gel was illuminated with a UV light. The gel pictures of several runs are shown in Fig.3.5. The first well was filled with DNA ladder to visually see the base pair length (bp) of the sample. The bands were observed between 200 and 300 bp and the target DNA is 260 bp in length. This result verifies the selective amplification of the target DNA.

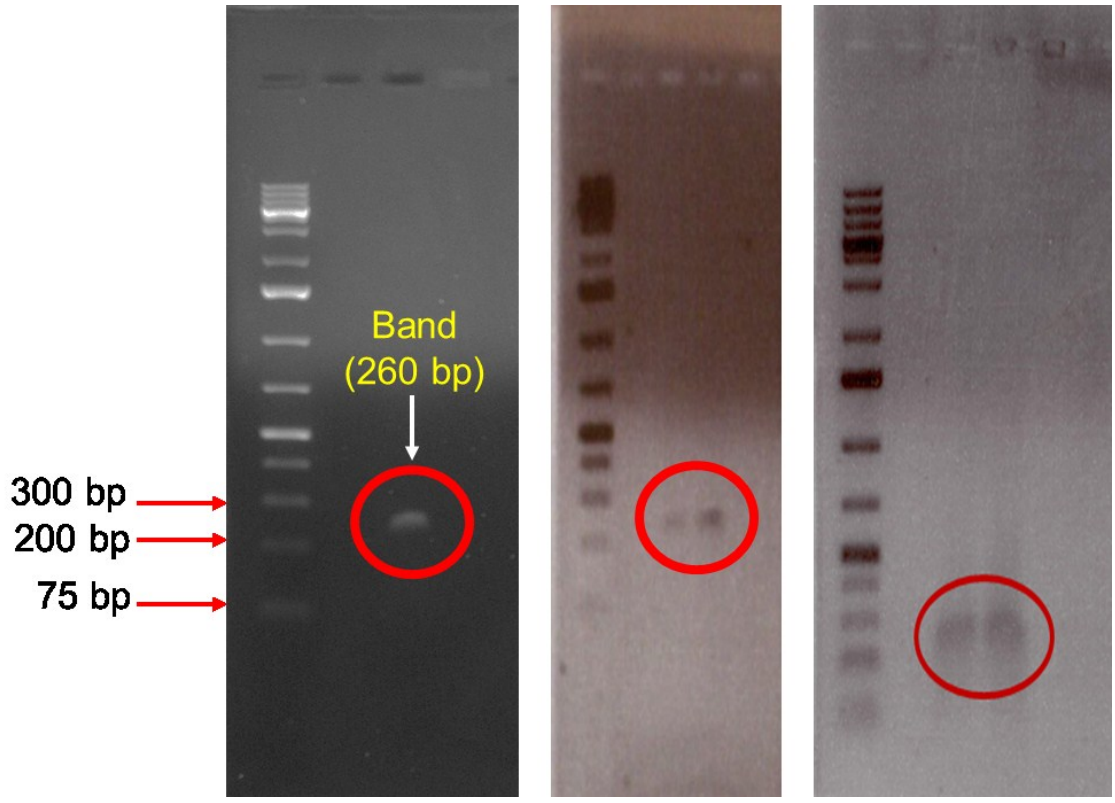

Fig. 3.5 Gel electrophoresis results of PCR runs. The bands are observed between 200 and 300 bp. The first well is filled with DNA ladder to aid in visualization of the bands

3.5.2 Evaluation of Repeatability and Success Ratio

The amplification of pure fungal genomic DNA was tested repeatedly to ensure proper functioning of the PADLOC system. Many PCR runs (10) were done and both PMT output voltages and gel electrophoresis results were compared. In all of the runs, bands were observed in correct location in gel electrophoresis. In most of the runs, fluorescence intensity detection using the PMT was also included. According to the results, in several of the runs the PMT voltage increase as the PCR cycles increased were

not significant. The problem is caused by inherent drift in PMT. As time passes by, the PMT outputs less voltage under the same conditions. The PMT can be warmed-up by applying voltage for a certain amount of time before the experiment starts to reduce the drift. In the PCR experiments, the PMT was used without warming up and caused drift in the output voltage.

The drift in PMT was characterized by measuring the PMT voltage while the chamber was empty. Without warming-up the PMT, the drift was found out to be around 8.75% at the end of the experiment. With a 60 minute warm-up period the drift dropped down to 1.5% at the end of the experiment. Under the light of these findings, it was concluded that the drop in PMT voltage was caused by the drift in PMT and this problem can be improved significantly by warming-up the PMT before the experiment.

3.6 Multichamber Design Results

The PCR experiment was tested using the serpentine design small chambers. All the conditions including sample preparation, BSA coating, cycle times, and optical housing integration were the same. There are two differences from big chamber design. They are additional autoclaved PDMS slabs inclusion to seal the inlet and outlet and the temperature values were different. The set temperatures were obtained in serpentine design calibration as mentioned in Section 2.5. The drift in the PMT was also taken into account as opposed to previous big chamber experiments. A PCR run using an empty chamber was done and the results were accounted to have a constant output. The values then were applied to PCR experiment. The resulting PMT output graph is shown in

Fig.3.6. Since the volume for the small chamber is small and we previously confirmed from big chamber designs that when we observe an increase in PMT output, we also observed a band in correct location in gel electrophoresis verification.

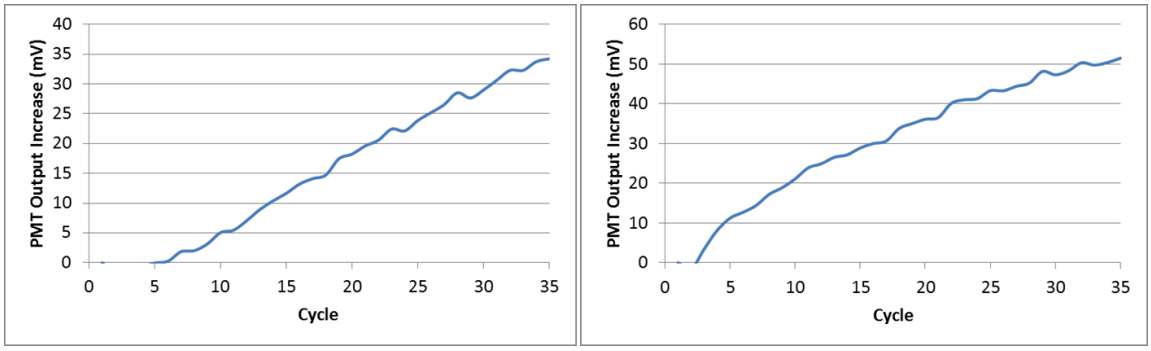

Fig. 3.6 The PMT output graphs of serpentine design. The increases in signal intensity are shown

The fluorescence intensities increased which was attributed to amplification of DNAs during the thermocycling.

CHAPTER IV

SUMMARY AND FUTURE WORK

4.1 Project Review

In this work, we developed and utilized a miniaturized real-time quantitative PCR system that can be used to diagnose plant pathogens.

The system is comprised of three sub-systems. The first sub-system is a microfabricated PCR chip to hold the PCR sample inside that is made of glass with gold layer on top to accomplish thermocycling of the sample. The second sub-system is a fluorescent intensity detector that employs LED, lenses, mirrors, dichroic mirror and PMT for fluorescent excitation and collection. The optical components are placed in a housing to ensure proper alignment of the components and avoid light leakage. The selection of LED as a light source and small PMT as an optical detector allows us to have a portable system with low power requirements. Lastly, the third system is NI Labview software and modules to read and display temperature and voltage data as well as control the temperature using PID control via a thermocouple.

The PCR chip has two different designs based on their high-throughput needs. A square spiral design was used to heat up a relatively large chamber that holds enough PCR sample to run gel electrophoresis and serpentine heater design was used to increase the high throughput of the system. Three serpentine heaters were placed in 25.4 x 25.4 mm PCR chip having three chambers. The designs were checked for uniform heating using COMSOL Multiphysics® software before fabricating. The optical detection

system is characterized before starting the PCR experiments using spectrophotometer for accurate and efficient excitation and emission wavelengths. Additionally, the optical detection system was characterized using increased concentrations of fluorescent dye that has similar characteristics as PCR sample.

The PADLOC system was tested using pure fungal genomic DNA that affects some crops such as tomato. The detection was done in real-time thanks to the optical system while thermocycling of the sample takes place. Additionally, for the big chamber design gel electrophoresis verification was done after the end of the experiment. Both PMT output voltage and gel electrophoresis results showed that our PADLOC system achieved detection of plant pathogen DNA.

4.2 Future Work

There are two aspects of our PADLOC system that can be advanced. These aspects are application side and device side. On the application side, the accomplishment of the PADLOC system has enabled further pathogen detection possible. In this work, the DNA used in the experiments was pure fungal genomic DNA. As future work, the target DNA will be changed to DNAs that are extracted from tomato plants. Those DNAs will have both tomato and fungal DNA if the plant is infected. The DNAs will be obtained from our collaborator Dr. Shim's lab. We believe the detection of extracted DNA will enable on-site detection thanks to the portability of our PADLOC system.

On the device side, the multiple chamber design has been run individually so far. The system will be modified to enable multiplex detection of three samples at the same time. For this goal, optical housing will be modified slightly. There will be three LEDs and three aspheric lenses to individually focus light into each chamber. The LEDs will turn on and off sequentially at the last seconds of extension zone. The filters, lenses and dichroic mirror will be kept the same. Thus, by employing the current setup as much as possible the optical system will be used for multiplex detection of PCR samples.

REFERENCES

1 Agriculture, U.S.D. *National Program 303: Plant Diseases*. 2010 [cited 2012; Available from: http://www.ars.usda.gov/research/programs/programs.htm?np_code=303&docid=12682.

2 R. K. Saiki, S. Scharf, F. Faloona, K. B. Mullis, G. T. Horn, H. A. Erlich and N. Arnheim ,*Science*, 1985. **230**(4732): p. 1350-1354.

3 F. C. Lawyer, S. Stoffel, R. K. Saiki, K. Myambo, R. Drummond and D. H. Gelfand , *Journal of Biological Chemistry*, 1989. **264**(11): p. 6427-6437.

4 C. J. Easley, L. A. Legendre, J. P. Landers and J. P. Ferrance, *Microchip Capillary Electrophoresis : Methods and Protocols*, 2006. **339**: p. 217-231.

5 R. Higuchi, G. Dollinger, P. S. Walsh and R. Griffith , *Bio-Technology*, 1992. **10**(4): p. 413-417.

6 C. A. Heid, J. Stevens, K. J. Livak and P. M. Williams, *Genome Research*, 1996. **6**(10): p. 986-994.

7 C. S. Zhang, J. L. Xu, W. L. Ma and W. L. Zheng, *Biotechnology Advances*, 2006. **24**(3): p. 243-284.

8 M. A. Northrup, M. T. Ching, R. M. White and R. T. Watson, *Tranducer'93 Seventh International Conference on Solid State Sens Actuators.* 1993. Yokohama, Japan.

9 A. T. Woolley, D. Hadley, P. Landre, A. J. deMello, R. A. Mathies and M. A. Northrup, *Analytical Chemistry*, 1996. **68**(23): p. 4081-4086.

10 R. C. Anderson, X. Su, G. J. Bogdan and J. Fenton,*Nucleic Acids Research*, 2000. **28**(12).

11 T. B. Taylor, E. S. WinnDeen, E. Picozza T. M. Woudenberg and M. Albin, *Nucleic Acids Research*, 1997. **25**(15): p. 3164-3168.

12 P. Belgrader, J. K. Smith, V. W. Weedn and M. A. Northrup, *Journal of Forensic Sciences*, 1998. **43**(2): p. 315-319.

13 S. Poser, T. Schulz, U. Dillner, V. Baier, J. M. Kohler, D. Schimkat, G. Mayer and A. Siebert, *Sensors and Actuators A-Physical*, 1997. **62**(1-3): p. 672-675.

14 M. U. Kopp, A. J. de Mello and A. Manz, *Science*, 1998. **280**(5366): p. 1046-1048.

15 P. Gascoyne, J. Satayavivad and M. Ruchirawat, *Acta Tropica*, 2004. **89**(3): p. 357-369.

16 J. West, B. Karamata, B. Lillis, J. P. Gleeson, J. Alderman, J. K. Collins, W. Lane, A. Mathewson and H. Berney, *Lab Chip*, 2002. **2**(4): p. 224-230.

17 J. Liu, M. Enzelberger and S. Quake, *Electrophoresis*, 2002. **23**(10): p. 1531-1536.

18 A. L. Markey, S. Mohr and P. J. R. Day, *Methods*, 2010. **50**(4): p. 277-281.

19 I. Kobayashi, K. Uemura and M. Nakajima, *Colloids and Surfaces A-Physicochemical and Engineering Aspects*, 2007. **296**(1-3): p. 285-289.

20 D. Braun, *Modern Physics Letters B*, 2004. **18**(16): p. 775-784.

21 M. Krishnan, V. M. Ugaz and M. A. Burns, *Science*, 2002. **298**(5594): p. 793-793.

22 M. Q. Bu, T. Melvin, G. Ensell, J. S. Wilkinson and A. G. R. Evans, *Journal of Micromechanics and Microengineering*, 2003. **13**(4): p. S125-S130.

23 J. El-Ali, I. R. Perch-Nielsen, C. R. Poulsen, D. D. Bang, P. Telleman and A. Wolff, *Sensors and Actuators A-Physical*, 2004. **110**(1-3): p. 3-10.

24 C. S. Liao, G. B. Lee, J. J. Wu, C. C. Chang, T. M. Hsieh, F. C.Huang and C. H. Luo, *Biosensors & Bioelectronics*, 2005. **20**(7): p. 1341-1348.

25 I. Rodriguez, M. Lesaicherre, Y. Tie, Q. B. Zou, C. Yu, J. Singh, L. T. Meng, S. Uppili, S. F.Y. Li, P. Gopalakrishnakone and Z. E. Selvanayagam, *Electrophoresis*, 2003. **24**(1-2): p. 172-178.

26 D. J. Sadler, R. Changrani, P. Roberts, C. F. Chou and F. Zenhausen, *Itherm 2002: Eighth Intersociety Conference on Thermal and Thermomechanical Phenomena in Electronic Systems, Proceedings*, 2002: p. 1025-1032.

27 Q. B. Zou, U. Sridhar, Y. Cheng and J. Singh, *Ieee Sensors Journal*, 2003. **3**(6): p. 774-780.

28 T. Fukuba, T. Yamamoto, T. Naganuma and T. Fujii, *Chemical Engineering Journal*, 2004. **101**(1-3): p. 151-156.

29 L. Erill, S. Campoy, J. Rus, L. Fonseca, A. Ivorra, Z. Navarro, J. A. Plaza, J. Aguilo and J. Barbe, *Journal of Micromechanics and Microengineering*, 2004. **14**(11): p. 1558-1568.

30 V. P. Iordanov, J. Bastemeijer, A. Bossche, P. M. Sarro, M. Malatek, I. T. Young, G. W. K. van Dedem and M. J. Vellekoop, *Proceedings of the Ieee Sensors 2003, Vols 1 and 2*, 2003: p. 1045-1048.

31 H. Yang, C. A. Choi, K. H. Chung, C. H. Chun and Y. T. Kim, *Analytical Chemistry*, 2004. **76**(5): p. 1537-1543.

32 A. Gulliksen, L. Solli, F. Karlsen, H. Rogne, E. Hovig, T. Nordstrom and R. Sirevag, *Analytical Chemistry*, 2004. **76**(1): p. 9-14.

33 P. J. Obeid and T.K. Christopoulos, *Analytica Chimica Acta*, 2003. **494**(1-2): p. 1-9.

34 Z. M. Zhou, D. Y. Liu, R. T. Zhong, Z. P. Dai, D. P. Wu, H. Wang, Y. G. Du, Z. N. Xia, L. P. Zhang, X. D. Mei and B. C. Lin, *Electrophoresis*, 2004. **25**(17): p. 3032-3039.

35 C. J. Bruckner-Lea, T. Tsukuda, B. Dockendorff, J. C. Follansbee, M. T. Kingsley, C. Ocampo, J. R. Stults and D. P. Chandler, *Analytica Chimica Acta*, 2002. **469**(1): p. 129-140.

36 Y. Matsubara, K. Kerman, M. Kobayashi, S. Yamamura, Y. Morita and E. Tamiya, *Biosensors & Bioelectronics*, 2005. **20**(8): p. 1482-1490.

37 M. W. Mitchell, X. Z.Liu, Y. Bejat, D. E. Nikitopodoulos, S. Soper and M. C. Murphy, *Microfluidics, Biomems, and Medical Microsystems*, 2003. **4982**: p. 83-98.

38 C. G. Koh, W. Tan, M. Q. Zhao, A. J. Ricco and Z. H. Fan, *Analytical Chemistry*, 2003. **75**(22): p. 6379-6379.

39 M. Curcio and J. Roeraade, *Analytical Chemistry*, 2003. **75**(1): p. 1-7.

40 P. Sethu and C. H. Mastrangelo, *Sensors and Actuators B-Chemical*, 2004. **98**(2-3): p. 337-346.

41 X. M. Yu, D. C. Zhang, T. Li, L. Hao and X. H. Li, *Sensors and Actuators A-Physical*, 2003. **108**(1-3): p. 103-107.

42 N. Krishnan, N. Agrawal, M. A. Burns and V. M. Ugaz, *Analytical Chemistry*, 2004. **76**(21): p. 6254-6265.

43 N. Y. Zhang, H. D. Tan and E. S. Yeung, *Analytical Chemistry*, 1999. **71**(6): p. 1138-1145.

44 A. F. R. Huhmer and J. P. Landers, *Analytical Chemistry*, 2000. **72**(21): p. 5507-5512.

45 J. P. Ferrance, Q. R. Wu, B. Giordano, C. Hernandez. Y. Kwok, S. Thibodeau and J. P. Sanders, *Analytica Chimica Acta*, 2003. **500**(1-2): p. 223-236.

46 D. Pal and V. Venkataraman, *Sensors and Actuators A-Physical*, 2002. **102**(1-2): p. 151-156.

47 K. Orrling, P. Nilsson, M. Gullberg and M. Larhed, *Chemical Communications*, 2004. **7**: p. 790-791.

48 C. Fermer, P. Nilsson and M. Larhed, *European Journal of Pharmaceutical Sciences*, 2003. **18**(2): p. 129-132.

49 R. M. Guijt, A. Dodge, G. W. K. van Dedem, N. F. de Rooij and E. Verpoorte, *Lab Chip*, 2003. **3**(1): p. 1-4.

50 S. Stern, C. Brooks, M. Strachan, A. Kopf-Sill and J. W. Parce, *Itherm 2002: Eighth Intersociety Conference on Thermal and Thermomechanical Phenomena in Electronic Systems, Proceedings*, 2002: p. 1033-1038.

51 W. C. Dunn, S. C. Jacobson, L. C. Waters, N. Kroutchinina, J. Khandurina, R. S. Foote, M. J. Justice, L. J. Stubbs and J. M. Ramsey, *Analytical Biochemistry*, 2000. **277**(1): p. 157-160.

52 J. Khandurina, T. E. McKnight, S. C. Jacobson, L. C. Waters, R. S. Foote and J. M. Ramsey, *Analytical Chemistry*, 2000. **72**(13): p. 2995-3000.

53 E. T. Lagally, J. R. Scherer, R. G. Blazej, N. M. Toriello, B. A. Diep, M. Ramchandani, G. F. Sensabaugh, L. W. Riley and R. A. Mathies, *Analytical Chemistry*, 2004. **76**(11): p. 3162-3170.

54 R. Drmanac, S. Drmanac, Z. Strezoska, T. Paunesku, I. Labat, M. Zeremski, J. Snoddy, W. K. Funkhouser, B. Koop, L. Hood and R. Crkvenjakov, *Science*, 1993. **260**(5114): p. 1649-1653.

55 R. H. Liu, J. N. Yang, R. Lenigk, J. Bonanno and P. Grodzinski, *Analytical Chemistry*, 2004. **76**(7): p. 1824-1831.

56 D. Trau, T. M. H. Lee, A. I. K. Lao, R. Lenigk, I. M. Hsing, N. Y. Ip, M. C. Carles and N. J. Sucher, *Analytical Chemistry*, 2002. **74**(13): p. 3168-3173.

57 H. Nagai, Y. Murakami, Y. Morita, K. Yokoyama and E. Tamiya, *Analytical Chemistry*, 2001. **73**(5): p. 1043-1047.

58 M. Krishnan, D. T. Burke and M. A. Burns, *Analytical Chemistry*, 2004. **76**(22): p. 6588-6593.

59 J. A. Higgins, S. Nasarabadi, J. S. Karns, D. R. Shelton, M. Cooper, A. Gbakima and R. P. Koopman, *Biosensors & Bioelectronics*, 2003. **18**(9): p. 1115-1123.

60 N. C. Cady, S. Stelick, M. V. Kunnavakkam and C. A. Batt, *Sensors and Actuators B-Chemical*, 2005. **107**(1): p. 332-341.

61 K. Sun, A. Yamaguchi, Y. Ishida, S. Matsuo and H. Misawa, *Sensors and Actuators B-Chemical*, 2002. **84**(2-3): p. 283-289.

62 Q. Xiang, B. Xu and D. Li, *Biomedical Microdevices*, 2007. **9**(4): p. 443-449.

63 M. A. Northrup, B. Benett, D. Hadley, P. Landre, S. Lehew, J, Richards and P. Stratton, *Analytical Chemistry*, 1998. **70**(5): p. 918-922.

64 Z. Zhao, Z. Cui, D. F. Cui and S. H. Xia, *Sensors and Actuators A-Physical*, 2003. **108**(1-3): p. 162-167.

65 Y. C. Lin, M. Li, M. T. Chung, C. Y. Wu and K. C. Young, *Sensors and Materials*, 2002. **14**(4): p. 199-208.

66 S. F. Li, D. Y. Fozdar, M. F. Ali, H. Li, D. B. Shao, D. M. Vykoukal, J. Vykoukal, P. N. Floriano, M. Olsen, J. T. McDevitt, P. R. C. Gascoyne and S. C. Chen, *Journal of Microelectromechanical Systems*, 2006. **15**(1): p. 223-236.

67 P. Belgrader, S. Young, B. Yuan, M. Primeau, L. A. Christel, F. Pourahmadi and M. A. Northrup, *Analytical Chemistry*, 2001. **73**(2): p. 286-289.

68 Y. J. Liu, C. B. Rauch, R. L. Stevens, R. Lenigk, J. N. Yang, D. B. Rhine and P. Grodzinski, *Analytical Chemistry*, 2002. **74**(13): p. 3063-3070.

69 Y. K. Cho, J. Kim, Y. Lee, Y. A. Kim, K. Namkoong, H. Lim, K. W. Oh, S. Kim, J. Han, C. Park, Y. E. Pak, C. S. Ki, J. R. Choi, H. K. Myeong and C. Ko, *Biosensors & Bioelectronics*, 2006. **21**(11): p. 2161-2169.

70 S. Julich, M. Riedel, M. Kielpinski, M. Urban, R. Kretschmer, S. Wagner, W. Fritzsche, T. Henkel, R. Moller and S. Werres, *Biosensors & Bioelectronics*, 2011. **26**(10): p. 4070-4075.

71 J. Kim and B. K. Gale, *The 10th International Conference on Miniaturized Systems for Chemistry and Life Sciences*. 2006. Tokyo, Japan.

72 K. J. Astrom and T. Hagglund, *Control Engineering Practice*, 2001. **9**(11): p. 1163-1175.

73 K. H. Ang, G. Chong, and Y. Li, *Ieee Transactions on Control Systems Technology*, 2005. **13**(4): p. 559-576.

APPENDIX A

COMSOL JOULE HEATING MANUAL

Overview

Joule Heating, also known as resistive heating is the phenomenon where a conductor releases heat when electric current goes through it.

Example: Temperature Profile of a Chamber

1. Open COMSOL by double-clicking its icon. When the "Model Wizard" opens, select a space dimension: 3D (Using 3D space produces the most accurate results but reduced dimensions can be used to save time and computation power).
2. In the "Add physic" window, click the heat transfer folder, then click "joule heating (jh)". Click the next arrow button.
3. In the "Select study type" window, you can choose stationary for the steady-state position or time dependent to see the physics in your model at the specified times. Then click the finish button.
4. Click "Geometry1" in the "Model builder" window, and change the length unit to an appropriate scale. (μm in this example)

Drawing

5. There are two different ways to make your model in Comsol. The first one is to draw your model in CAD software and save as .dxf file. You can import your model into Comsol by right clicking "Geometry1" and import. Right

after the import you can use the “zoom extents” button on the “Graphics” toolbar to see the whole design in appropriate scale. After importing, you can extrude and finish the design forming union. (Will be described) In the case of having to use a complicated design, it is better draw the design in a CAD software and import to Comsol since Comsol without CAD module is not very user-friendly and has limited geometry selections.

6. To draw a microchamber device consisting of a patterned and etched glass sheet and a glass sheet with Au electrode on top, right click to “Geometry1” and select work plane and click build selected on top toolbar. Now the drawing panel is ready when you go to “Geometry” under the “Geometry1” menu on the left part of the screen. Click “draw square (center)” and enter the value of 25400 μm as side length, x, 0 μm, and y, 0 μm as center coordinates. Right-click “Geometry1” and click “rectangle” and enter the value of Width, 20000 μm, Height, 5000 μm, x, -10000 μm, and y, 5000 μm for the corner. Then, add two “square (center)” with the side length of 1000 μm. The center coordinates are y, 7500 μm and x, 10500 and -10500 μm. For the chamber part, click “ellipse (center)” and use the values a-semi axis, 6000 μm, b-semi axis, 2000 μm, x, 0 μm and y, 7500 μm.

7. After drawing all the shapes, it is time to give the objects third dimension which can be done by extruding and using Boolean operations. Right click the work plane and select extrude, select the eclipse check the reverse direction to extrude in the other direction and enter 80 μm.

8. Right click on the work plane and select extrude again. Select the square and extrude 500 μm in reverse direction.
9. In the same fashion, select the remaining shapes (three rectangles) and extrude 600 μm. (In regular direction)
10. In the work plane, draw the same square (25400 μm side length) that was drawn first (Explained in step 6). It may be harder to select this square if it is drawn before extrusion processes so that is the reason why it is drawn now. Extrude this 500 μm.
11. Right click "Geometry1" and select Boolean operation ➔ Difference. In the "Objects to add" include the three rectangles while in the "Objects to subtract" select the "sq4" that is the last square drawn. Click build selected and this will create a hanging electrode design.
12. Draw a square identical to "sq4" and extrude 500 μm to have a complete design.
13. Click "Form Union" to finalize your drawing. Alternatively, you can use "Form Assembly" to have a manual control on the boundaries and the physics. However, forming union is a convenient and more automated approach. The finalized drawing is shown below.

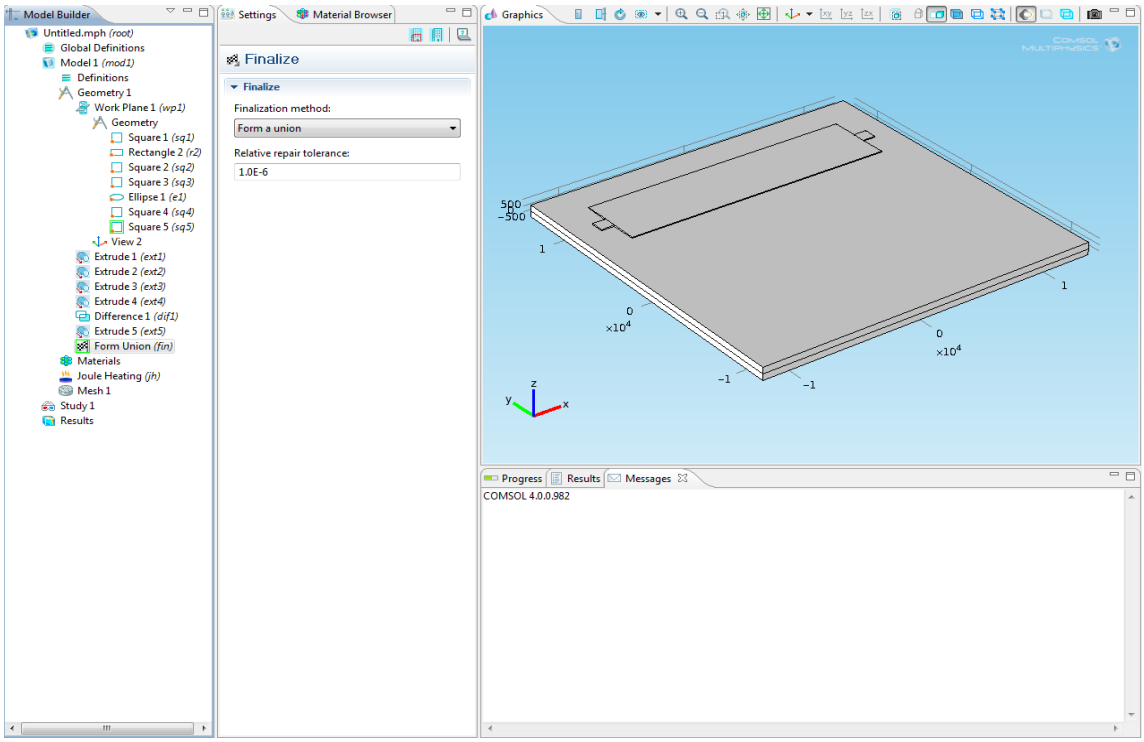

Fig. A.1 Finalized Drawing of Heater

Materials

14. Now that we have a complete drawing, we can assign materials to the drawings. For this purpose, locate the "Model builder" window, right-click "Materials" and select "Open Material Browser"

15. In the "Material Browser", expand the "Built-in" folder, locate Silica Glass, right-click and select "Add Material to Model"

16. Select domain 1 and 2 by first left clicking and then right clicking. The blue color means the material has been applied to the highlighted domains.

17. Add gold the selection to domain 3, 4 and 6. Under the "Material Content" part a stop sign on the left of the relative permittivity is shown. Put 1 here and

it turns into a green tick. Green tick means the value is ok, the stop sign means the value is not valid and computation cannot be done.

18. To add material properties, click the material name under the material folder; expand “Material Properties” in the “Material” window. Click “Basic properties” and right-click the property which you want to add and select “add to material”.

19. Finally, add water to selection and apply to domain 5. It cannot be seen directly so you can press transparency button on the upper toolbar to have a transparent drawing and you can select the domain 5. Use 80 as relative permittivity of water. The material assignment is now finished and ready for physics assignment.

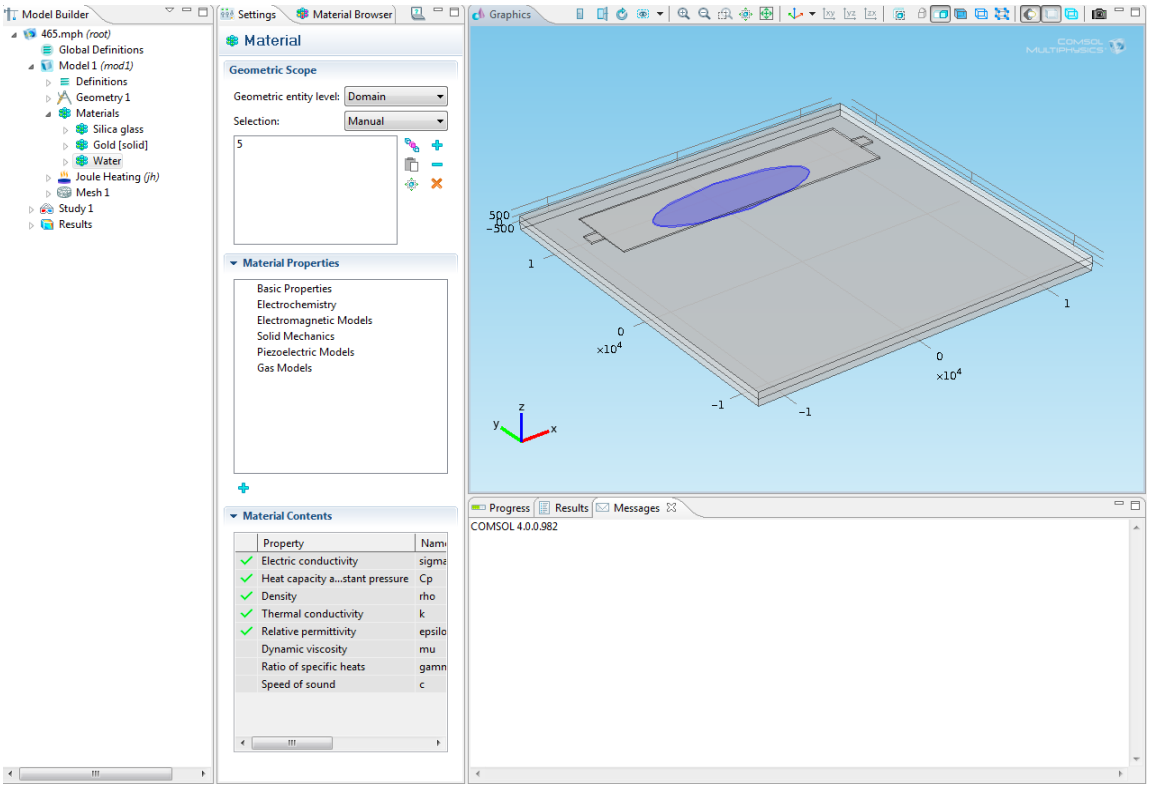

Fig. A.2 Finalized Drawing of Microdevice

Physics

20. In the “Model Builder”, expand the “Joule Heating” node.

21. Right click on “Joule Heating” and select “Heat Transfer ➔ Heat Flux” on the second part of the drop-down menu. This is the part where the affected domains can be set. In our case all the boundaries except for the ground and electric voltage applied boundaries will be affected. In the upper part of middle menu, choose all boundaries and manually remove the domains 10 and 35. In the bottom part, click inward heat flux and use 10 as heat transfer coefficient.

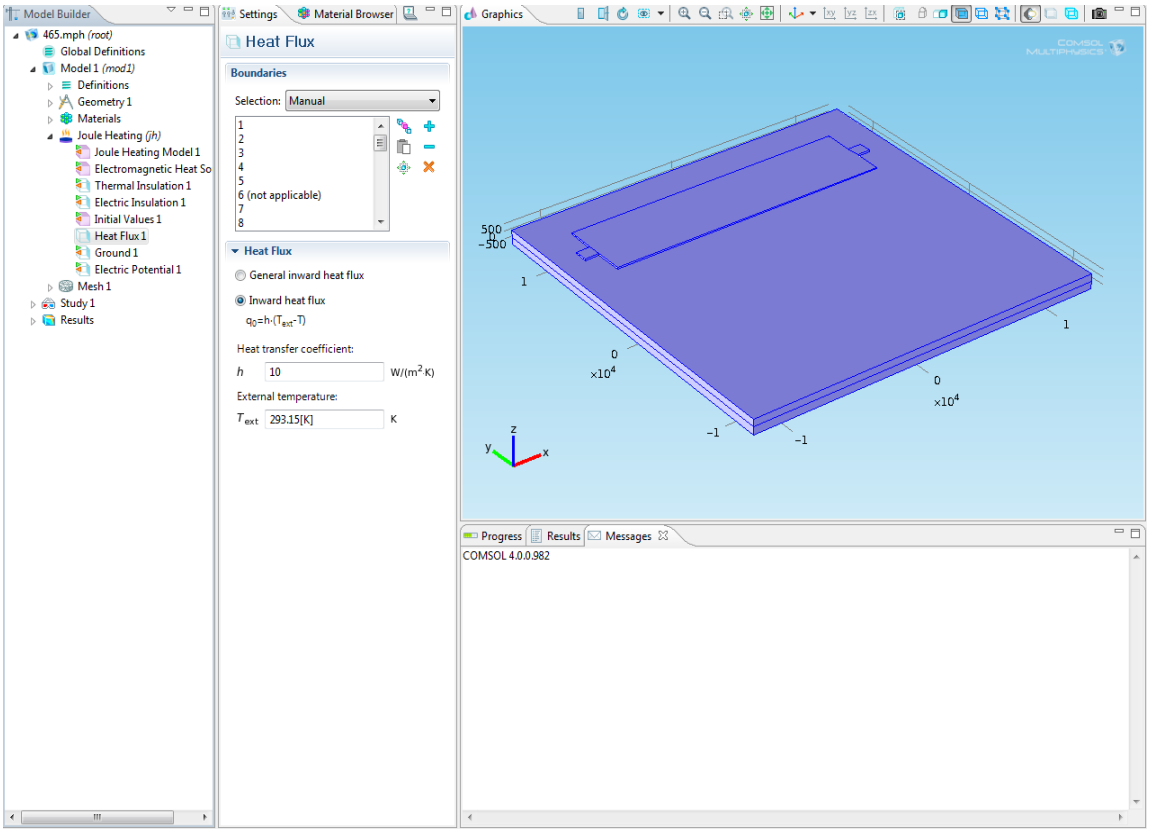

Fig. A.3 Application of Heat Flux

22. Right-click the "Joule Heating" in the "Model Builder", click "Electric Currents ➔ Ground" and select domain 10. This is where your ground will be.

23. Right-click the "Joule Heating" in the "Model Builder", click "Electric Currents ➔ Electric Potential" and select domain 35. Enter the applied voltage here as 0.04 V

Meshing

24. Click "Mesh" In the "Model Builder", select "Element size" and choose coarse. Right click "Free Tetrahedral" and choose "Build All" to complete

meshing. Coarse meshing has fewer elements than normal so it takes less time to compute. However, it is important to note that the accuracy drops as you have coarser meshing.

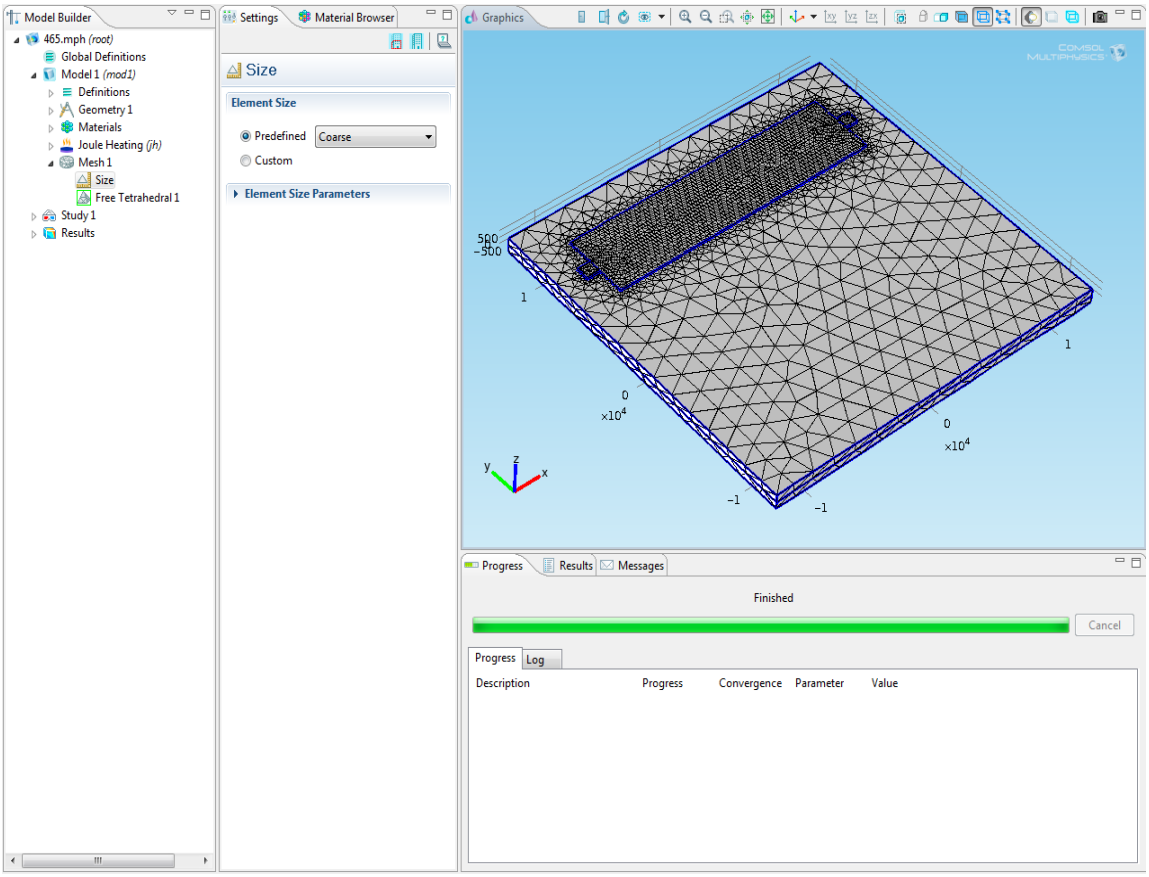

Fig. A.4 Structure of the Device After Meshing

Study

25. To run a stationary simulation, right-click “study I” in the “Model Builder” and choose “Compute”.

26. On the other hand, if you are running a time-dependent simulation, click "study I" to expand and locate "Step 1: Time Dependent". Click the button next "Times" where you can select the start time, stop time and interval in seconds. Afterwards, right-click "study I" in the "Model Builder" and choose "Compute"

Results

27. Under "Results"➔"3D Pilot Group1", click the "Surface1". In the "Settings" window, click "Range" and select "Manual color range" to see the desired interval on the surface.

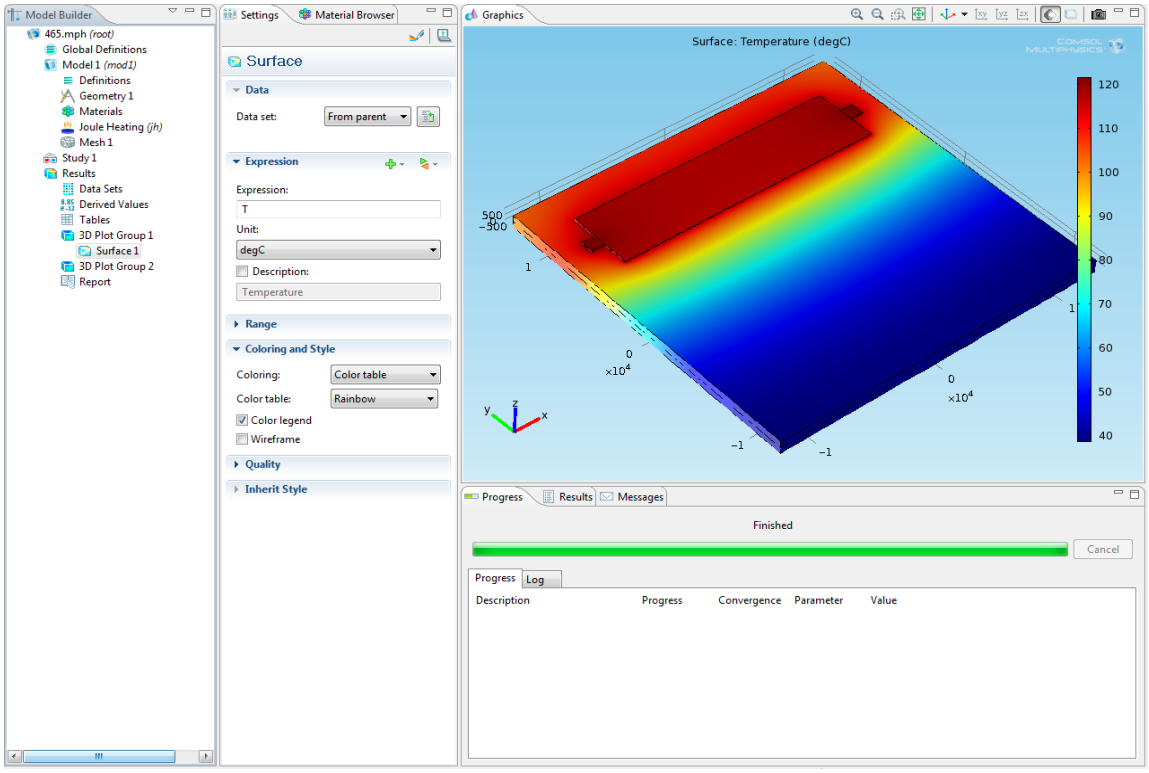

Fig. A.5 3D Overview of Simulation

28. To see the cross section of the chamber, go to “3D Group2” and select the slice. On the right menu, under “plane data” the cut direction can be chosen. Afterwards, a number of equally spaced planes or an exact coordination plane can be sliced. The cross-section of the chamber is shown below.

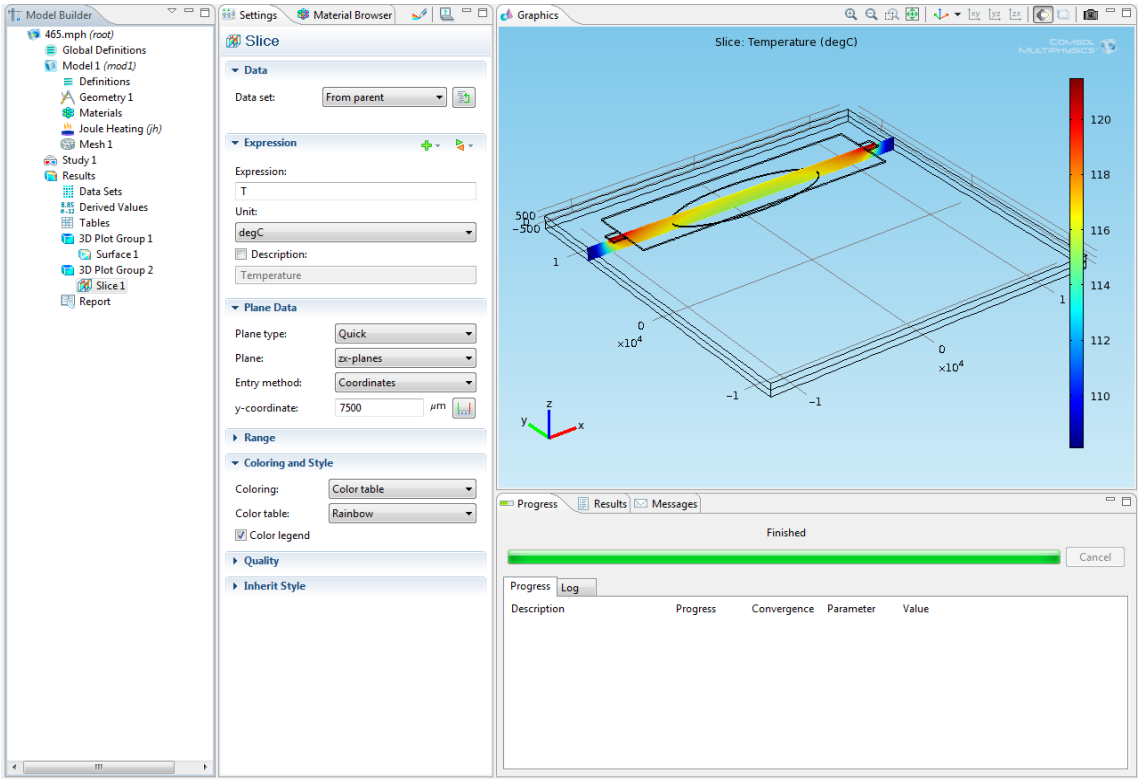

Fig. A.6 Cross-section View of the Chamber

APPENDIX B

LABVIEW PROGRAM

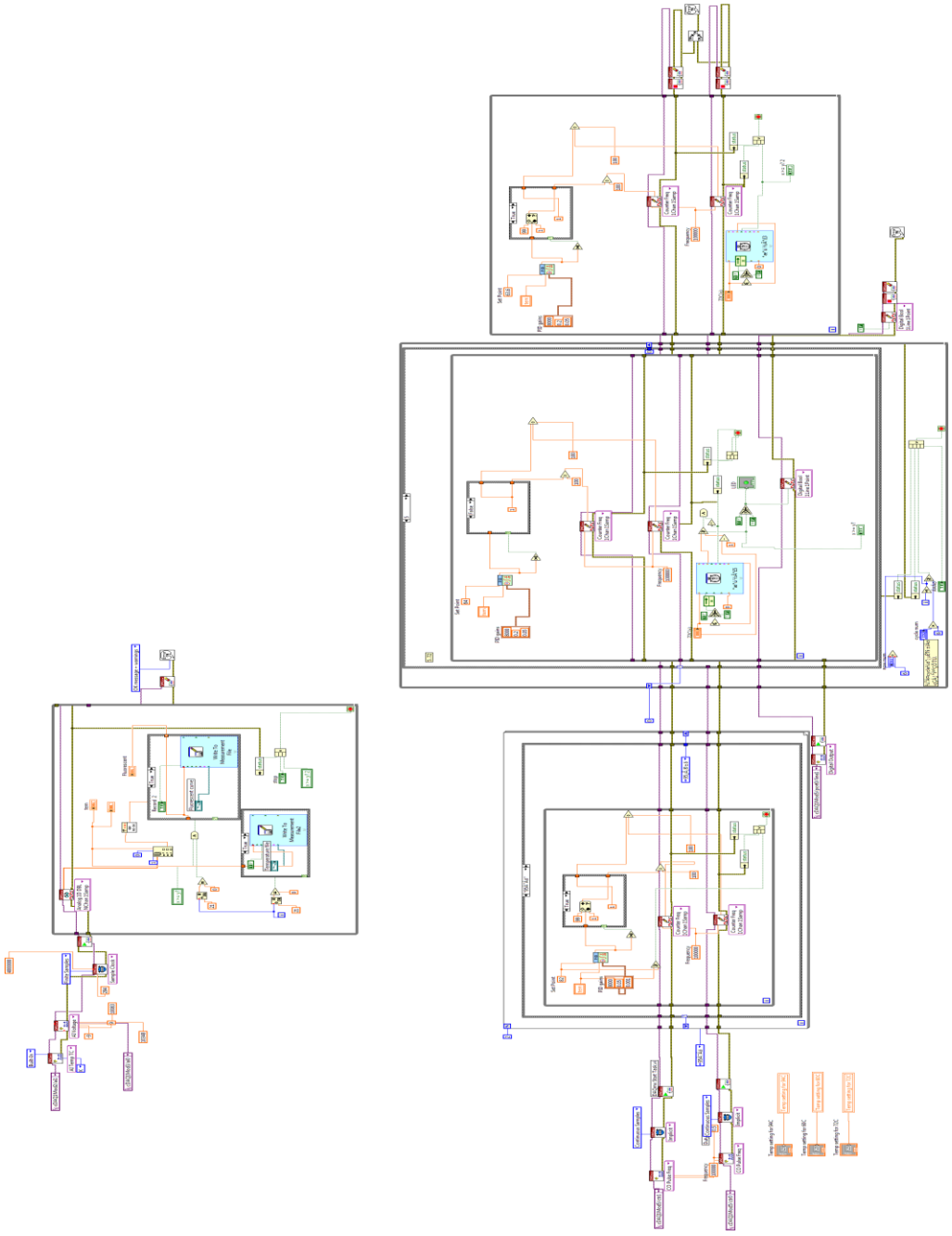

Fig. B.1 Labview program used in PADLOC project (pcr program_122111.vi)

APPENDIX C

MASK DESIGNS FOR HEATERS AND CHAMBERS

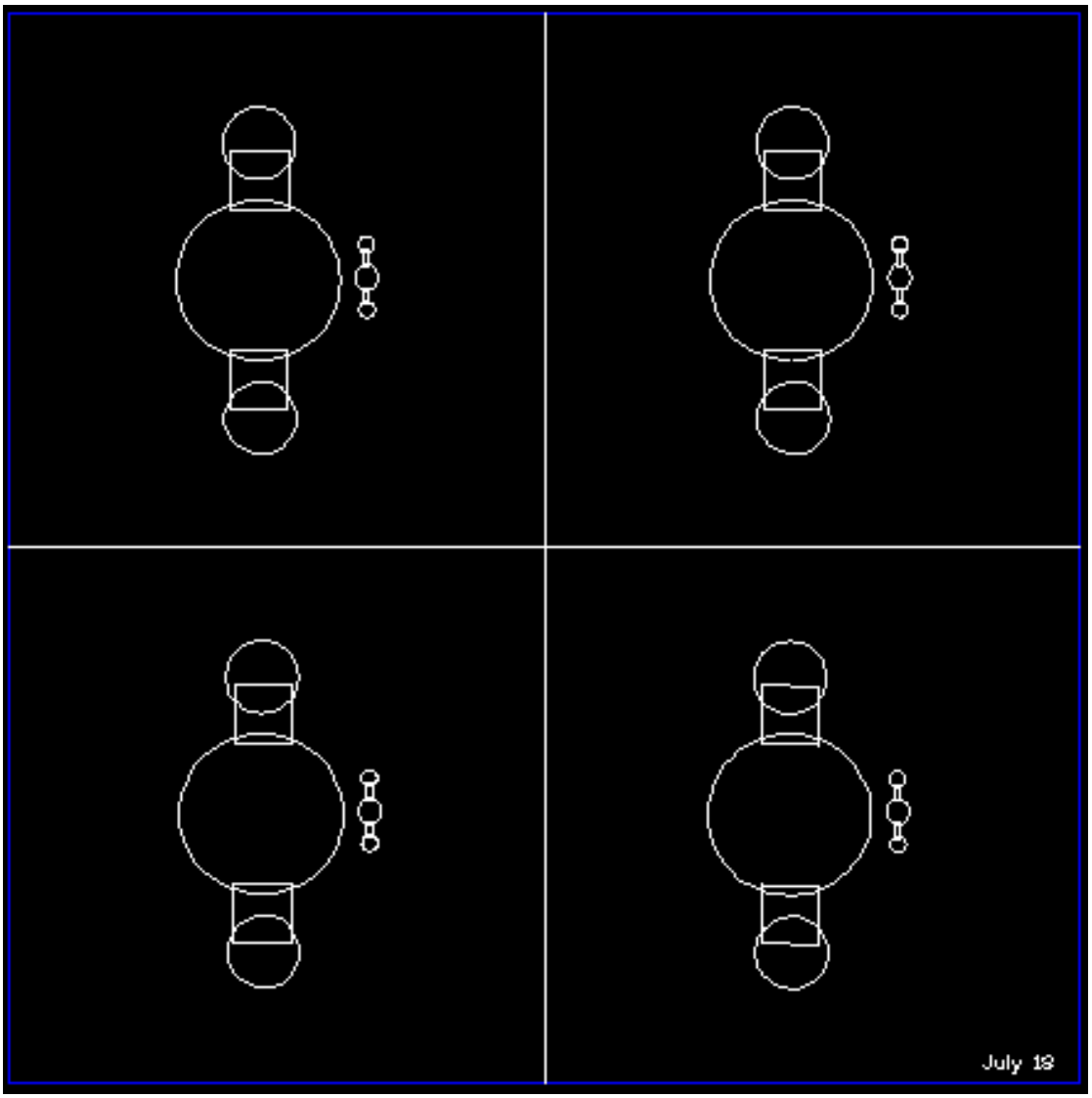

Fig. C.1 Big chamber design (Big chamber July 18 Glass chip.dwg)

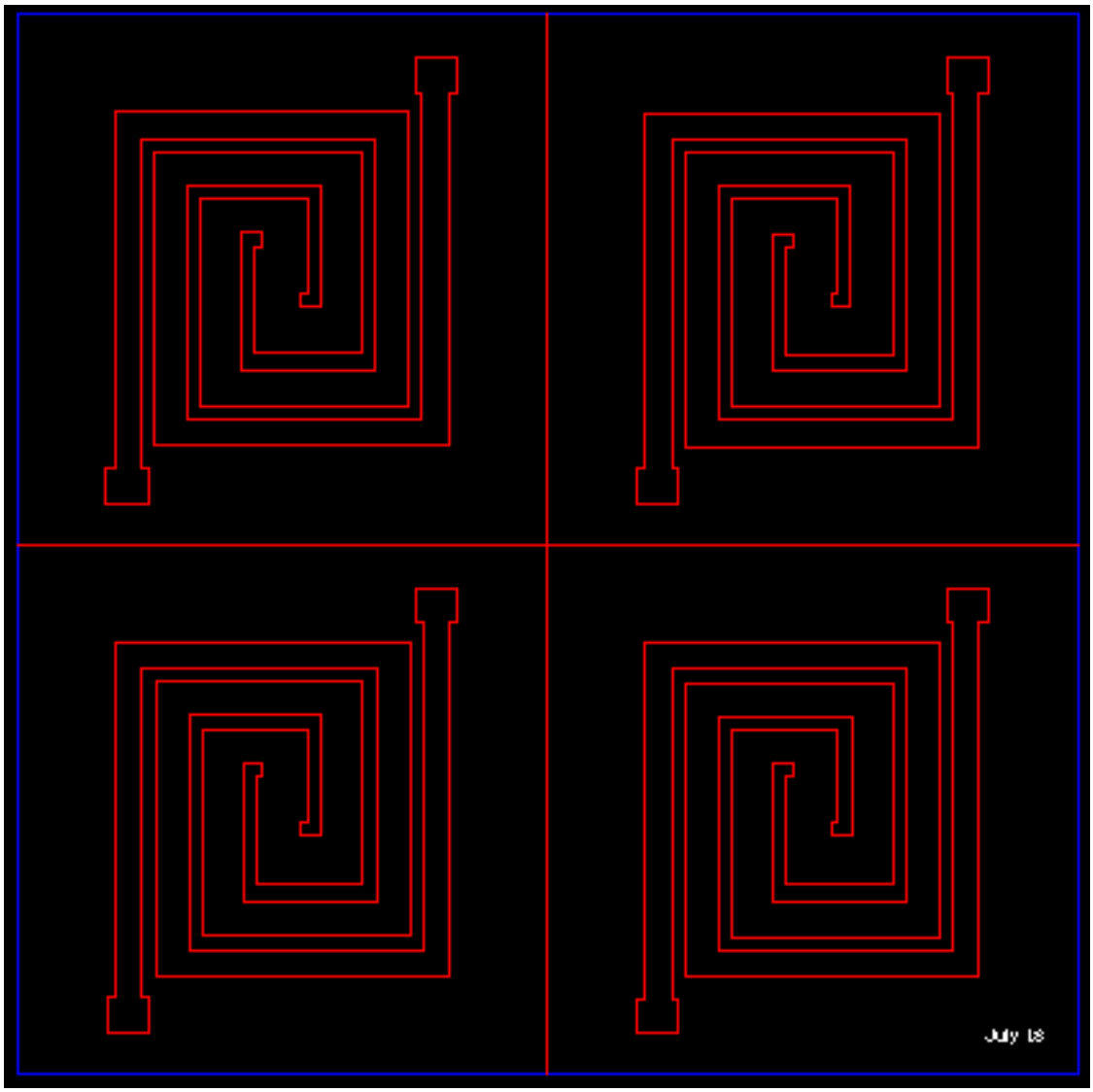

Fig. C.2 Big heater design (Heater_July 18.dwg)

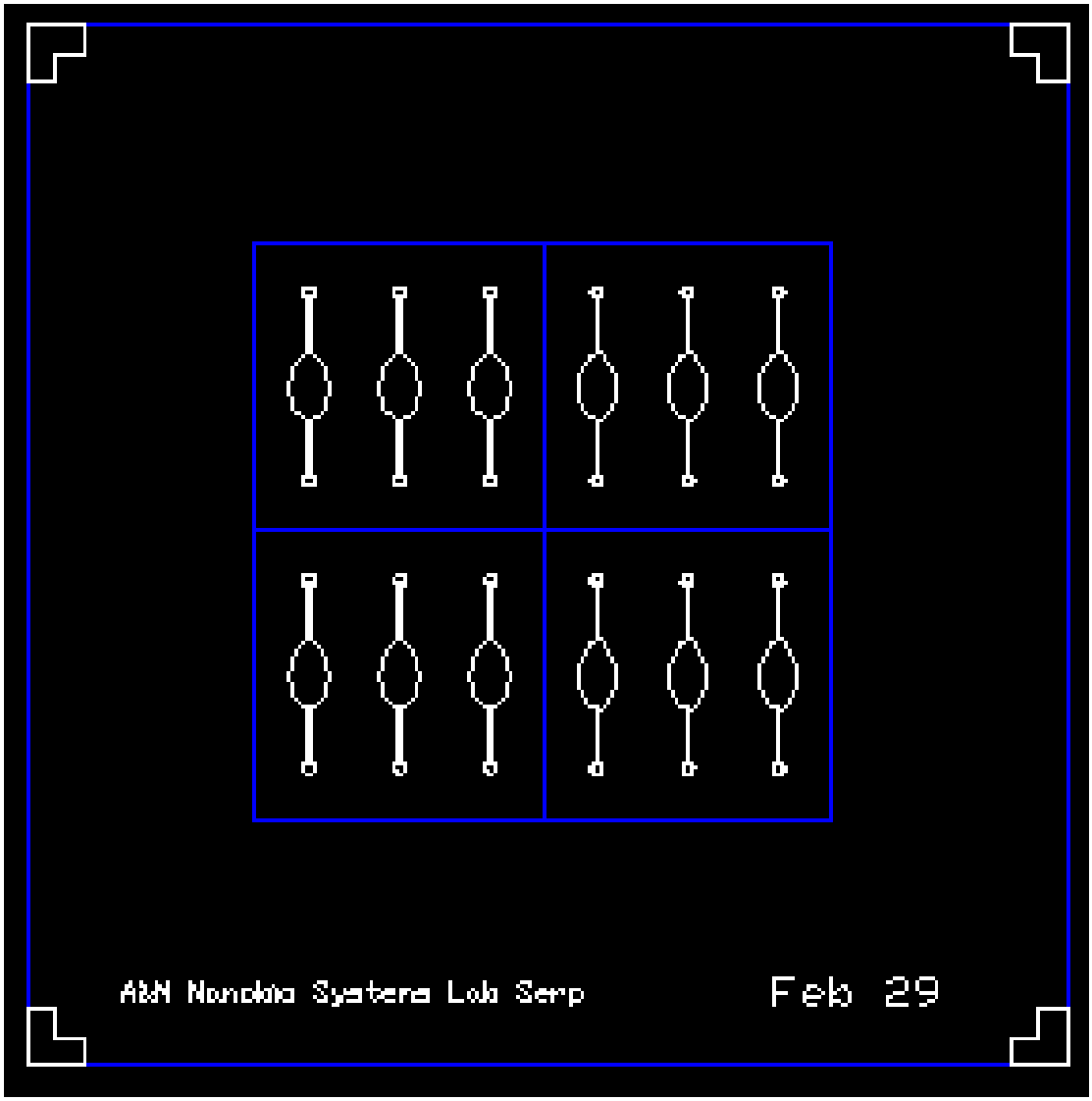

Fig. C.3 Serpentine design chamber (Feb 29 Modified heater+chambers.dwg)

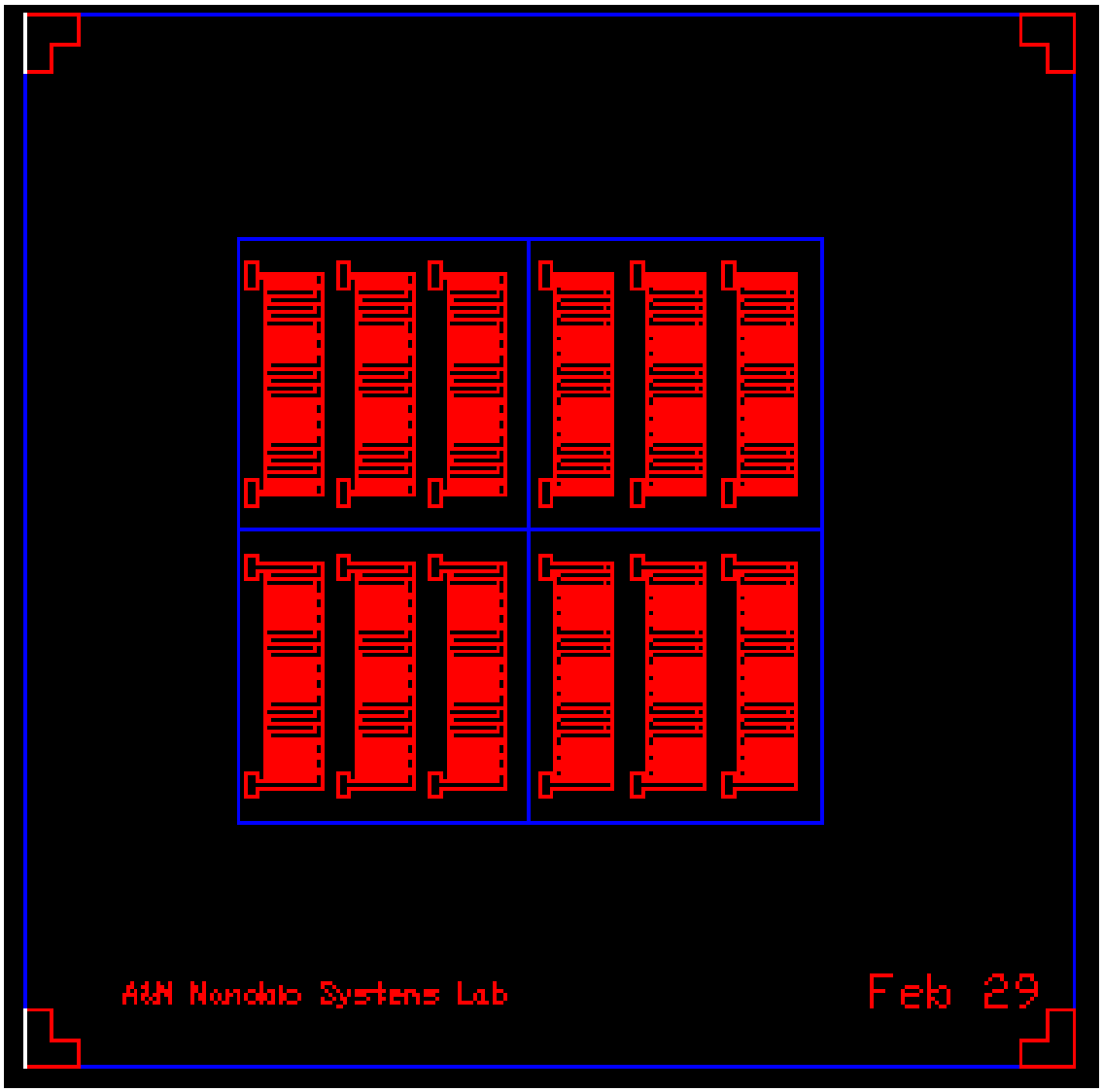

Fig. C.4 Serpentine design heater design (Feb 29 Modified heater+chambers.dwg)

APPENDIX D

MICROFABRICATION PROCEDURES

Microchamber Fabrication Procedure

1. Clean the 2-inch square glass slide using piranha solution (H_2SO_4:H_2O_2 = 3:1 (v/v)) for 20 minutes and then thoroughly rinse with deionized (DI) water and dry with nitrogen gas.
2. Deposit Cr and Au layer using an E-beam evaporator to thickness of 180/1000 Angstrom.
3. Spin-coat photoresist (Microposit® S1818, Rohm-Haas-Shipley Company, Inc., Marlborough, MA, USA) onto the wafer at 4000 rpm for 30 sec with an acceleration of 5.
4. Soft bake the wafer at 110°C for 4 minutes.
5. Load the wafer to mask aligner (Karl Suss MA6 Mask Aligner, SUSS Microtec, Inc., Waterbury Center, VT, USA) and expose to UV light for a dose of 87 mJ/cm^2.
6. Develop the photoresist using the developer (Microposit® MF-319, Rohm-Haas14 Shipley Company, Inc., Marlborough, MA, USA) for about 1 minute.
7. Etch to the desired pattern using first gold and then chromium etchant.
8. Tape (MicroAmp® Optical Adhesive Covers, Applied Biosystems, Beverly, MA, USA) the back side of the slide to avoid etching the back side of the glass.

9. Prepare HF solution ((49%HF (J.T. Baker):H_2O = 5:1 (v/v))) and etch the glass for around 19 minutes to achieve 80 μm depth.
10. Remove the tape and etch the cover mask using gold and chromium etchant.
11. Cut the samples in four (There are four patterns in one glass slide) with Professional Laser Series (PLS) 6.120D Laser Engraving and Cutting System (Universal Laser Systems, Inc., Scottsdale, AZ, USA) using 50% power and 10% speed.
12. Drill the inlet and outlet holes using the drill. Before drilling, apply CristalBond™ 509 (West Chester, PA, USA) wax to avoid cracks in the glass.

Heater Fabrication Procedure

1. Clean the 2-inch square glass slide using piranha solution (H_2SO_4:H_2O_2 = 3:1 (v/v)) for 20 minutes and then thoroughly rinse with deionized (DI) water and dry with nitrogen gas.
2. Deposit Cr and Au layer using an E-beam evaporator to thickness of 200/2000 Angstrom.
3. Spin-coat photoresist (Microposit® S1818, Rohm-Haas-Shipley Company, Inc., Marlborough, MA, USA) onto the wafer at 4000 rpm for 30 sec with an acceleration of 5.
4. Soft bake the wafer at 110°C for 4 minutes.

5. Load the wafer to mask aligner (Karl Suss MA6 Mask Aligner, SUSS Microtec, Inc., Waterbury Center, VT, USA) and expose to UV light for a dose of 87 mJ/cm^2.
6. Develop the photoresist using the developer (Microposit® MF-319, Rohm-Haas14 Shipley Company, Inc., Marlborough, MA, USA) for about 1 minute.
7. Etch to the desired pattern using first gold and then chromium etchant.
8. Cut the samples in four (There are four patterns in one glass slide) with Professional Laser Series (PLS) 6.120D Laser Engraving and Cutting System (Universal Laser Systems, Inc., Scottsdale, AZ, USA) using 50% power and 10% speed

VITA

Osman Safa Cifci received his Bachelor of Science degree in Electrical Engineering from Eskisehir Osmangazi University in 2009. He entered the Electrical Engineering program at Texas A&M University in August 2010. His research interests include miniaturization for life sciences applications.

Mr. Cifci may be reached at 214 Zachry Engineering Center TAMU 3128 College Station, TX 77843-3128. His email is osmansafa@tamu.edu.